2020-11-02

ATF-4 and hydrogen sulfide signalling mediate longevity from inhibition of translation or mTORC1 [preprint]

Cyril Statzer
Swiss Federal Institute of Technology in Zurich

Et al.

ATF-4 and hydrogen sulfide signalling mediate longevity from inhibition of translation or mTORC1

Cyril Statzer[1], Richard Venz[1], Monet Bland[2,3], Stacey Robida-Stubbs[2,3], Jin Meng[2,3], Krina Patel[2,3], Raffaella Emsley[4], Dunja Petrovic[5], Pengpeng Liu[6], Ianessa Morantte[7], Cole Haynes[6], Milos Filipovic[5], William B. Mair[7], Alban Longchamp[4], T. Keith Blackwell[2,3*], and Collin Y. Ewald[1*]

1 Eidgenössische Technische Hochschule Zürich, Department of Health Sciences and Technology, Institute of Translational Medicine, Schwerzenbach-Zürich CH-8603, Switzerland

2 Department of Genetics, Harvard Medical School, Boston, Massachusetts, United States

3 Joslin Diabetes Center, Research Division, Boston, Massachusetts, United States

4 Department of Vascular Surgery, Centre Hospitalier Universitaire Vaudois and University of Lausanne, Lausanne, Switzerland

5 Leibniz-Institut für Analytische Wissenschaften-ISAS-e.V., Dortmund, Germany

6 Department of Molecular, Cell and Cancer Biology, University of Massachusetts Medical School, Worcester, MA, U.S.A.

7 Department of Genetics and Complex Diseases, Harvard School of Public Health, 665 Huntington Avenue, Boston, MA 02115, U.S.A.

*Corresponding authors: collin-ewald@ethz.ch (C.Y.E.) and keith.blackwell@joslin.harvard.edu (T.K.B.)

Keywords: mRNA translation, cystathionine gamma-lyase, H_2S, ageing, mTORC1, Integrated Stress Response, *C. elegans*

Abstract

Inhibition of mTORC1 (mechanistic target of rapamycin 1) slows ageing, but mTORC1 supports fundamental processes that include protein synthesis, making it critical to elucidate how mTORC1 inhibition increases lifespan. Under stress conditions, the integrated stress response (ISR) globally suppresses protein synthesis, resulting in preferential translation of the transcription factor ATF-4. Here we show in *C. elegans* that the ATF-4 transcription program promotes longevity and that ATF-4 upregulation mediates lifespan extension from mTORC1 inhibition. ATF-4 activates canonical anti-ageing mechanisms but also increases expression of transsulfuration enzymes to promote hydrogen sulfide (H_2S) production. ATF-4-induced H_2S production mediates longevity and stress resistance from *C. elegans* mTORC1 suppression, and ATF4 drives H_2S production in mammalian dietary restriction. This H_2S boost increases protein persulfidation, a protective modification of redox-reactive cysteines. Increasing H_2S levels, or enhancing mechanisms that H_2S modulates through persulfidation, may represent promising strategies for mobilising therapeutic benefits of the ISR or mTORC1 inhibition.

Introduction

Over the last three decades, genetic and phenotypic analyses of ageing have revealed the paradigm that across eukaryotes, lifespan can be extended by inhibition of mechanisms that promote growth and proliferation [1–7]. Prominent among these is the kinase complex mTORC1, which coordinates a wide range of growth-related processes in response to growth factor and nutrient signals [2–4]. mTORC1 activity can be reduced by dietary restriction (DR), or by pharmacological interventions such as rapamycin, an mTORC1 inhibitor that increases lifespan from yeast to mice [2,3,6,7]. However, DR is challenging to maintain and not entirely beneficial for health, and while rapamycin represents an exciting paradigm for anti-ageing pharmacology, mTORC1 suppression has wide-ranging effects on the organism [2,3,6,7]. Rapamycin is used clinically as an immunosuppressant, and mTORC1 broadly affects metabolism and supports the synthesis of proteins, nucleic acids, and lipids. Elucidation of specific mechanisms through which mTORC1 influences longevity is critical not only for understanding the biology of ageing and longevity, but also the development of molecularly targeted anti-ageing therapies that maintain health.

Because of its short lifespan and amenability to genetics, the nematode *C. elegans* has been invaluable for identifying mechanisms that promote longevity. In *C. elegans*, suppression of translation initiation increases both lifespan and stress resistance [8–13]. Work in *C. elegans* and *Drosophila* indicates that lifespan extension from mTORC1 inhibition is mediated in part through a global reduction in mRNA translation [14,15]. A mechanistic understanding of how mRNA translation levels affect longevity will therefore provide mechanistic insights into how mTORC1 inhibition increases lifespan.

Suppression of new protein synthesis is an important mechanism through which cells protect themselves under stressful conditions that include nutrient deprivation, and thermal-, oxidative-, and endoplasmic reticulum (ER) stress [8–13]. Under these conditions, certain protective proteins are translated preferentially. In the integrated stress response (ISR), stress conditions induce a broad reduction in cap-dependent mRNA translation by activating kinases that phosphorylate and inhibit the translation initiation factor subunit eIF-2α [16–18]. This suppression of translation leads in turn to preferential translation of the activating transcription factor ATF4, which coordinates various stress defense mechanisms to reestablish homeostasis [16–18]. ATF4 also increases expression of amino acid biosynthesis genes, and in mammalian cell culture experiments mTORC1 promotes ATF4 translation through its broad upregulation of protein synthesis [19–21]. This last result seems paradoxical, given that ATF4 synthesis is increased when translation is suppressed in the ISR, but is logical given the need to maintain amino acid levels under conditions of high growth activity.

Here we have investigated whether and how ATF4 and the ISR might influence longevity. In *C. elegans*, we find that ATF4 is essential for longevity arising from inhibition of protein synthesis and, importantly, is a pro-longevity factor that extends lifespan when overexpressed on its own. ATF-4 increases lifespan by enhancing canonical anti-aging mechanisms, but also transsulfuration enzyme-mediated hydrogen sulfide (H_2S) production. The anti-aging benefits of mTORC1 suppression depend upon ATF-4 activation, which in turn increases levels of H_2S and protein persulfidation, an H_2S-induced protective modification of redox-reactive cysteine (Cys) residues. Dietary restriction (DR) acts through ATF-4 to increase H_2S in mammals,

68 suggesting conservation of ATF-4 as a longevity mediator. The data identify ATF-4
69 as a pro-longevity factor and suggest that in living animals ATF-4 regulation by
70 mTORC1 is more complex than currently appreciated. They also suggest that
71 increasing H_2S levels, or enhancing processes that H_2S modulates through
72 persulfidation, may represent a promising strategy for mobilising specific therapeutic
73 benefits of the ISR, mTORC1 inhibition or DR.
74

Results

ATF-4 responds to translation suppression to increase C. elegans *lifespan*

We investigated whether *C. elegans atf-4* is regulated similarly to mammalian ATF4 at the level of mRNA translation. In mammals 2-3 small upstream open reading frames (uORFs) within the ATF4 5' untranslated region (UTR) occupy the translation machinery under normal conditions, inhibiting translation of the downstream ATF4 coding region [19,22,23]. By contrast, when eIF-2α phosphorylation impairs translation initiation, the uORFs are bypassed, and ATF4 is translated preferentially. The *C. elegans atf-4* ortholog (previously named *atf-5*) contains two 5' UTR uORFs (Fig. 1a; Extended Data Fig. 1a, 1b), deletion of which increases translation of a transgenic reporter [23], predicting that translation of the *atf-4* mRNA will be increased under conditions of global translation suppression.

We tested this idea in *C. elegans* that express green fluorescent protein (GFP) driven by the *atf-4* upstream region, including the uORFs (P*atf-4*(uORF)::GFP, Fig. 1a, 1b). P*atf-4*(uORF)::GFP expression was extremely low under unstressed conditions, but was increased dramatically by translation suppression or conditions that elicit the ISR, including ER stress from treatment with tunicamycin (TM) or DTT (Fig. 1b, Extended Data Fig. 1c, 1d). By contrast, TM treatment increased *atf-4* mRNA levels only 1.5-fold (Fig. 1d, Extended Data Fig. 1e). The increase in P*atf-4*(uORF)::GFP fluorescence arising from ER stress was not prevented when transcription was blocked by alpha-amanitin (Fig. 1d, 1e), further indicating post-transcriptional regulation, supporting the idea that the endogenous *atf-4* locus is regulated similarly, while the ATF-4 mRNA was expressed at steady levels during development and ageing (Extended Data Fig. 1f). Ribosomal profiling demonstrated

that during development, when overall translation levels are high, ribosome occupancy was enriched on the endogenous *atf-4* uORFs compared to the coding region (Fig. 1f). We conclude that, like mammalian ATF4, *C. elegans atf-4* is preferentially translated upon conditions of reduced protein synthesis (Extended Data Fig. 1g).

Our data suggest that in *C. elegans*, genetic or pharmacologic suppression of mRNA translation can serve as a proxy method of activating ATF-4 that would bypass stress induction of the ISR Accordingly, a low dose of the translation elongation blocker cycloheximide increased P*atf-4*(uORF)::GFP expression (Fig. 1b, Extended Data Fig. 1c, 1d). Because ATF-4 is upregulated by translation suppression, we hypothesised that it might mediate the accompanying lifespan extension. Lifespan of *C. elegans* can be increased by RNA interference (RNAi) to various translation initiation factors (*ifg-1*/eIF4G, *ife-2*/eIF4E, or *eif-1A*/eIF1AY), as reported previously [8–13], but this extension was abrogated in *atf-4(tm4397)* loss-of-function mutants (Fig. 1g, Supplementary Table 1). Similarly, a low dose of cycloheximide extended the lifespan of wild type (WT) but not *atf-4(tm4397)* animals (Fig. 1h, Supplementary Table 1). Thus, preferential translation of *atf-4* is required for lifespan extension from a global reduction in cytoplasmic protein synthesis.

ATF-4 mobilises canonical pro-longevity mechanisms

In *C. elegans*, a limited number of transcription factors have been identified that can increase lifespan when overexpressed (including DAF-16/FOXO, HSF-1/HSF1, and SKN-1/NRF)[1,24]. These evolutionarily conserved regulators are generally associated with enhancement of protective mechanisms such as stress resistance, protein folding or turnover, and immunity. To determine whether ATF-4 can actually

promote longevity, as opposed to being required generally for health, we investigated whether an increase in ATF-4 levels might extend lifespan. Transgenic ATF-4-overexpressing (ATF-4OE) animals exhibited nuclear accumulation of ATF-4 in neuronal, hypodermal, and other somatic tissues under unstressed conditions (P*atf-4*::ATF-4(cDNA)::GFP; Extended Data Fig. 2a). TM treatment doubled their ATF-4 protein levels (Extended Data Fig. 2b, Supplementary Data File 1), indicating that this ATF-4 transgene responds to environmental and physiological conditions. Importantly, ATF-4 overexpression (OE) increased lifespan by 7-44% across >10 independent trials, which included two experiments without FuDR and analysis of independent transgenic lines (Fig. 2a, Supplementary Table 1). ATF-4 OE also prolonged healthspan (Fig. 2b, Extended Data Fig. 2c Supplementary Table 2). Thus, the elevated activity of the ATF-4 transcriptional program is sufficient to extend lifespan and promote health.

To identify longevity-promoting mechanisms that are enhanced by ATF-4, we used RNA sequencing (RNA-seq) to compare gene expression profiles in *atf-4* loss-of-function or ATF-4OE animals to WT under non-stressed conditions (Fig. 2c, Extended Data Fig. 3a-d, Supplementary Table 3). Only a modest number of genes were detectably up- or down-regulated by *atf-4* loss or OE, respectively (Fig. 2c, Extended Data Fig. 3c-d). Notably, ATF-4 OE upregulated several small heat shock protein (HSP) genes that are also controlled by HSF-1/HSF (heat shock factor) and DAF-16/FOXO (Fig. 2c), and are typically induced by longevity-assurance pathways [25,26]. Translation of *atf-4* was increased within minutes by a heat shock (Extended Data Fig. 3f, 3g), suggesting that ATF-4 functions in tandem with HSF-1/HSF1, and each of the ATF-4-upregulated chaperone genes *hsp-16.2*/HSPB1, *sip-1*/CRYAA,

hsp-70/HSPA1L, and *hsp*-4/BiP was required for lifespan extension from ATF-4 OE (Fig. 2d; Extended Data Fig. 3e; Supplementary Table 1). Together, the data suggest that ATF-4 enhances proteostasis mechanisms that have been linked to longevity.

Other findings further linked ATF-4 to longevity-associated mechanisms. ATF-4 OE increased expression of the cytoprotective gene *nit-1*/Nitrilase (Fig. 2d), a canonical target of the xenobiotic response regulator SKN-1/NRF [27], along with expression of collagen genes that are typically upregulated by SKN-1/NRF in response to lifespan extension interventions (Fig. 2c) [25]. The 3kb predicted promoter regions of many ATF-4-upregulated genes included not only the binding consensus for mammalian ATF4 (-TGATG-) [28,29], but also sites for DAF-16, HSF-1, and SKN-1 (Fig. 2d, Supplementary Table 4, 5). Furthermore, many genes that were upregulated by ATF-4 OE had been detected in chromatin IP (ChIP) analyses of these last three transcription factors (Extended Data Fig. 3h, Supplementary Table 5). Each of those transcription factors is critical for lifespan extension arising from suppression of translation [11,12], and we determined that they are also needed for long life conferred by ATF-4 OE (Fig. 2e, Supplementary Table 1). ATF-4 OE also robustly upregulated two adenine nucleotide translocase genes (ANT; *ant-1.3* and *ant-1.4,* Fig. 2c). The ANT complex is important for transport of ATP from the mitochondrial space into the cytoplasm, as well as for mitophagy [30], and both *ant-1.3* and *ant-1.4* were required for ATF-4 OE longevity (Fig. 2f, Supplementary Table 1). Together, our findings suggest that while the transcriptional impact of ATF-4 may seem limited in breadth, it cooperates with other longevity factors to enhance the activity of multiple mechanisms that protect cellular functions, thereby driving lifespan extension.

ATF-4 increases lifespan through H_2S production

To identify ATF-4-regulated genes that are conserved across species and might be particularly likely to have corresponding roles in humans, we queried our ATF-4OE vs WT RNA-seq results and compared the top 200 significantly upregulated *C. elegans* genes against 152 mammalian genes that are thought to be regulated directly by ATF4 [31]. Seven orthologues of these genes were upregulated by ATF-4 OE in *C. elegans* (Fig. 3a, Supplementary Table 4), four of which encoded components of the reverse transsulfuration (hereafter referred to as transsulfuration) pathway (*cth-2*/CTH), or associated mechanisms (*glt-1*/SLC1A2, *C02D5.4*/GSTO1 and *F22F7.7*/CHAC1; Fig. 3b, Supplementary Table 4). The transsulfuration pathway provides a mechanism for utilising methionine to synthesise cysteine and glutathione when levels are limiting [32], but the CTH enzyme (cystathionine gamma-lyase, also known as CGL and CSE) also generates H_2S as a direct product. Underscoring the potential importance of the H_2S-generating enzyme CTH-2 for ATF-4 function, the levels of its mRNA and protein were each increased by ATF-4 OE (Fig. 3c-e, Supplementary Data File 2).

Reduced methionine levels [33] and higher H_2S levels [34,35] have been linked to longevity. However, we did not detect any differences in the relative abundance of amino acids between ATF-4oe and WT animals (Supplementary Table 6), suggesting that ATF-4 is unlikely to influence longevity by altering amino acid levels. By contrast, ATF-4 OE consistently increased H_2S levels in a *cth-2*-dependent manner (Fig. 3f, Extended Data Fig. 4a-e). The increases in longevity and stress resistance that are conferred by ATF-4 OE were each fully abolished by *cth-2* knockdown (Fig. 3g, 3h, Supplementary Table 1, 7), suggesting that the increase in H_2S production that derived

from CTH-2 upregulation is a critical aspect of ATF-4 function. Given that the ISR results in preferential translation of ATF-4 [22,36], we asked whether ER stress conditions increase H_2S production. We found that treating WT animals with tunicamycin resulted in higher H_2S levels (Fig. 3i), suggesting that increased H_2S production is in general a part of the ISR. Taken together, our results show that the ISR and ATF-4 act at multiple levels to promote stress resistance and longevity, and that a CTH-2-driven increase in H_2S production is a critical aspect of this program (Fig. 3j).

Given that *atf-4* is essential for lifespan to be extended in response to reduced translation rates, we investigated whether *atf-4* and its transsulfuration target gene *cth-2* might be generally required for *C. elegans* lifespan extension. Although ATF4/ATF-4 has been implicated in responses to mitochondrial stress or protein synthesis imbalance [28,29], *atf-4* was dispensable for the increases in lifespan or oxidative stress resistance that follow from developmental impairment of mitochondrial function (Fig. 4a, Extended Data Fig. 4f, 4e Supplementary Table 1, 8). The extent of lifespan extension by reduced insulin/IGF-1 signalling or germ cell proliferation was decreased by *atf-4* mutation but did not depend upon *cth-2*, perhaps consistent with other transsulfuration components and H_2S producers being implicated in the latter pathway (Fig. 4b, 4c, Supplementary Table 1) [37]. We conclude that ATF-4 and the ISR may be indispensable for upregulating H_2S production and other longevity-promoting mechanisms specifically when lifespan extension is driven by a reduction in protein synthesis (Fig. 3j).

Longevity from mTORC1 suppression is driven by ATF-4, H_2S, and protein persulfidation

Because mTORC1 inhibition increases lifespan in part by reducing protein synthesis [14,15], our findings in Fig. 1 suggest that ATF-4 might be involved. mTORC1 is required for *C. elegans* larval development [2], but *C. elegans* lifespan can be increased by RNAi knockdown of mTORC1 signalling components during adulthood or by mutation of *raga-1*, which encodes one of the RAG GTPases (RAGA-1 and RAGC-1) that transduce amino acid signals to activate mTORC1 [2,3,6,7]. The former strategy allows mTORC1 activity to be reduced without any associated developmental effects. Knockdown of either RAG gene increased P*atf-4(uORF)*::GFP expression in living *C. elegans*, indicating that in *C. elegans* ATF-4 is preferentially translated when mTORC1 activity is reduced (Fig. 4d, Supplementary Table 9), as would be predicted by the decrease in mRNA translation that accompanies mTORC1 inhibition in *C. elegans* [13,14]. Importantly, the increases in lifespan extension, stress tolerance, and healthspan that resulted from loss of either *raga-1* or *ragc-1* function required *atf-4* (Fig. 4e-h, Extended Data Fig. 2c, 4g, Supplementary Table 1-2, 7, 8, 10), indicating that ATF-4 plays an essential role in the benefits of reducing mTORC1 activity *in vivo*.

Having determined that *atf-4* is required for mTORC1 suppression to extend lifespan, we were surprised to find that *atf-4* was dispensable for lifespan extension from rapamycin treatment, even though rapamycin increased ATF-4 translational reporter expression (Extended Figure 5a-d, Supplementary Table 1, 9). Notably, the mTOR kinase is present not only in mTORC1, but also within the mTORC2 complex [2,3]. mTORC2 is not as well understood as mTORC1, but it functions in growth signalling and its activation involves binding to the ribosome, suggesting an association with translation regulation (Extended Data Fig. 5a) [38]. Rapamycin mechanistically inhibits mTORC1, but continuous rapamycin treatment depletes the

mTOR kinase, thereby reducing mTORC2 activity [39]. We therefore investigated the possible involvement of *atf-4* in mTORC2 effects.

The effects of mTORC2 on *C. elegans* lifespan are complex, but adulthood RNAi knockdown of the essential mTORC2 subunit RICT-1 (Rictor) extends lifespan [14,40–42]. Knockdown of *rict-1* increased P*atf-4*(uORF)::GFP expression, suggesting an effect on translation, and the resulting lifespan extension required *atf-4* (Fig. 4i, Extended Figure 5c, Supplementary Table 1, 9). Consistent with earlier evidence that rapamycin impairs both mTORC1 and mTORC2 in *C. elegans* [14], simultaneous knockdown of *raga-1* (mTORC1) and *rict-1* (mTORC2) extended lifespan independently of *atf-4* (Extended Data Fig. 5e, Supplementary Table 1). Evidently, simultaneous mTORC1 and mTORC2 inhibition triggers mechanisms that obviate the requirement for *atf-4* that is observed when each mTOR kinase complex is inactivated separately.

We investigated whether mTOR inhibition might extend lifespan through an ATF-4-mediated increase in H_2S production (Fig. 3). Genetic inhibition of either mTORC1 or mTORC2 increased H_2S levels in an *atf-4*-dependent manner (Fig. 5a, 5b, Extended Data Fig. 5g, 5h). Furthermore, the ATF-4 target gene *cth-2* was fully required for the increased heat stress resistance and longevity of animals with impaired mTORC1 (Fig. 5c, 5d, Supplementary Table 1, 7), suggesting that this H_2S production is essential. Our findings show that reduced mTOR signalling leads to preferential translation of ATF-4, which increases cystathionine gamma lyase expression and H_2S to promote stress resilience and healthy ageing.

An important consequence of increased H_2S levels is an increase in protein persulfidation (SSH) at cysteine (Cys) thiols (SH) [37,43,44]. Redox modification and signalling at Cys residues are critical in growth signalling and other fundamental processes [43,44]. Under oxidising conditions, thiols that are prone to redox-reactivity can be converted to sulfenic acid (SOH), a modification that can proceed to irreversible and potentially damaging redox forms (SO_2H, SO_3H) [43,44]. H_2S converts SOH to SSH (persulfidation), a readily reversible modification that promotes stress resistance by protecting proteins and their functions [43,44].

PSSH levels can be visualised with chemoselective probes in a gel-based assay that reveals individual protein species, or by confocal microscopy [37]. In *C. elegans* PSSH levels are decreased by mutation of the *cth-2* paralog *cth-1*, suggesting that they are dependent upon a background level of H_2S produced by the latter [37]. By contrast, neither *atf-4* nor *cth-2* mutations globally altered PSSH, consistent with ATF-4-CTH-2 functioning largely as an inducible pathway of H_2S production, although *cth-2* appeared to be needed for appropriate levels of persulfidation of some individual proteins and in certain tissues (Fig. 5e, Supplementary Video 1, 2). PSSH levels were lower in *raga-1* mutants (reduced mTORC1 activity; Fig. 5e), possibly because mTORC1 inhibition is associated with increased antioxidant activities [14,45] that might reduce the levels of protein-SOH precursor. Interestingly, in the *raga-1* background *atf-4* mutation dramatically decreased PSSH levels across numerous different proteins (Fig. 5e), indicating that ATF-4 is a major regulator of protein persulfidation in the setting of low mTORC1 activity. Our data suggest that mTORC1 inhibition alters the overall balance of redox signalling in the organism, with ATF-4-induced H_2S production playing a crucial role in maintaining the levels and extent of PSSH.

ATF-4- induced H_2S production during mammalian DR

We investigated whether the ATF4-CTH pathway is involved in dietary restriction (DR), an intervention that extends lifespan in essentially all eukaryotes. Both a reduction in mTORC1 activity and an increase in H_2S have been implicated in mediating DR benefits [2,7,35,37,46]. In *C. elegans*, *atf-4* was not required for lifespan to be extended by a liquid culture food-dilution DR protocol, and was only partially required for lifespan extension in the genetic DR-related model *eat-2* (Fig. 6a, Supplementary Table 1). However, transsulfuration pathway genes other than *cth-2* are also partially required for *eat-2* lifespan extension [35,37], suggesting that in *C. elegans* multiple pathways might increase H_2S production during DR.

In mammals, restriction of sulfur-containing amino acids (Met and Cys) acts through ATF4 and CTH to boost endothelial H_2S levels and angiogenesis [47], and multiple longevity interventions increase CTH mRNA levels [48], suggesting a possible role for the ATF4-CTH pathway in DR. Supporting this idea, our bioinformatic analysis revealed that CTH mRNA levels were increased in various mouse tissues by DR (32/36 profiles), rapamycin (4/6 profiles), and growth hormone insufficiency (8/8 profiles) (Fig. 6b, Supplementary Table 11). To examine the role of ATF4 in DR directly, we subjected 12-week-old control or *ATF4* knockdown mice to a week of either DR or ad libitum (AL) feeding. ATF4 knockdown resulted in dramatically decreased levels of both basal and DR-induced H_2S production in the liver (Fig. 6c). Taken together, our data suggest that in mammals ATF4 is a major determinant of H_2S production during DR. They also predict that ISR/ATF4-induced H_2S upregulation

is likely to be an essential contributor to longevity in the setting of DR, mTOR suppression, and possibly other longevity interventions (Fig. 6d).

Discussion

We have determined that *C. elegans* lifespan can be extended by the ISR regulator ATF-4 and that ATF-4 enhances longevity and health in part by boosting H_2S production. Conditions that inhibit mRNA translation, including mTORC1 inhibition, increase ATF-4 expression and cannot extend lifespan in its absence. Previous studies revealed that longevity arising from inhibition of translation initiation depends upon preferential translation of protective genes [49], and increased transcription of stress defence genes [11,14]. Our new findings link these mechanisms by revealing that preferentially translated ATF-4 cooperates with DAF-16/FOXO, HSF-1/HSF, and SKN-1/NRF to drive protective gene transcription. The ATF-4-related protein Gcn4 contributes to DR longevity in *S. cerevisiae* [50], and we have found that ATF4 drives H_2S production in mammalian DR (Fig. 6c), suggesting that ATF-4 mediates an ancient protective program that promotes longevity.

Our evidence that reduced mTORC1 activity promotes longevity by increasing ATF-4 levels contrasts with mammalian evidence that pharmacological mTORC1 inhibition reduces ATF4 translation [19–21]. However, those findings were obtained in cultured cells that were also exposed to growth factors or had mTORC1 activated genetically, a very different scenario from adult *C. elegans*, in which growth has largely ceased and most tissues are post-mitotic. Consistent with our *C. elegans* results, in mouse liver ATF4 protein levels are increased in long-lived models, including rapamycin treatment and nutrient restriction [51], and mTORC1 hyperactivation (TSC1

deletion) decreases *CTH* expression and prevents DR from increasing *CTH* mRNA levels [35]. It will be interesting in the future to determine how mammalian mTORC1 influences ATF4 *in vivo* under a variety of conditions, including analysis of tissues with different levels of growth and mTORC1 activity.

We found that when mTORC1 activity is reduced, ATF-4 exerted its effects in part by increasing transsulfuration-mediated H_2S production, thereby globally increasing PSSH levels. This broad shift in posttranslational protein modification could influence many biological functions, including the activity of redox-regulated signalling pathways, making it of great interest to elucidate how these modifications influence the downstream effects of mTORC1 signalling. Although inhibition of mTORC1 has received widespread enthusiasm as an anti-ageing strategy, mTORC1 controls fundamental processes that include protein synthesis, mRNA splicing, autophagy, and metabolic pathways [2,3,7,52–54]. Similarly, although pharmacological inhibition of the ISR promotes memory and cognition by allowing protein synthesis [18,55], ISR suppression could reduce levels of H_2S, which has been shown to prevent neurodegeneration [56]. In these and other settings targeted mobilisation of beneficial mechanisms that are activated by ATF-4, including H_2S production, might be of promising long-term value. Consistent with this notion, H_2S confers many cardiovascular benefits in mammals, including a reduction in blood pressure [47,57–59], and patients suffering from vascular diseases show reduced CTH and H_2S levels [60], prompting clinical trials of H_2S-releasing agents for cardiovascular conditions (NCT02899364 and NCT02278276). It could be of considerable value to examine the potential benefits of ATF4 and H_2S in various settings, including prevention of ageing-related phenotypes and disease.

Author contributions

All authors participated in analysing and interpreting the data. C.Y.E. and T.K.B. designed the experiments. C.Y.E., K.P., M.B., S.R.S., C.S., and R.V. performed lifespan assays. C.Y.E., MB, C.S., and R.V. performed oxidative stress assays. C.Y.E., M.B., and C.S. performed thermotolerance assays. C.Y.E., MB, K.P., S.R.S., and R.V. scored GFP reporters. C.S., R.E., J.M., and A.L. performed H_2S capacity assay. P.L. and C.H. performed Ribosequencing analysis. D.P. and M.F. performed persulfidation assays and analysis. C.S. and C.Y.E. analysed transcription profiles. C.Y.E., C.S., J.M. performed qRT-PCR. R.V. performed the western bots. I.M. and W.B.M. generated transgenic strains. C.Y.E. performed all other assays. C.Y.E. and T.K.B. wrote the manuscript in consultation with the other authors.

Author Information

The authors have no competing interests to declare. Correspondence should be addressed to C. Y. E. and T.K.B.

Acknowledgement

We thank Alex Hofer, Sara Schütze, Carolin Imse, Julia Rogers, and Lorenza E. Moronetti Mazzeo for help with scoring lifespan, stress, and GFP assays, Michael Steinbaugh for help with the initial analysis of the RNA sequencing data, Stephanie Lin for contributing to earlier stages of this work, S. Mitani and the National BioResource Project for the *atf-4(tm4212* and *tm4397)* alleles, Mike Crowder for the *rars-1(gc47)* allele, Chi Yun and David Ron for the P*atf-4*(uORF)::GFP reporter strain, Jay Mitchell and Nancy Pohl for comments on the manuscript, and Spalentor and Michael Hall for inspiration. Some strains were provided by the CGC, which is funded

399 by the NIH Office of Research Infrastructure Programs (P40 OD010440). Portions of
400 this research were conducted on the Orchestra High Performance Computer Cluster
401 at Harvard Medical School (NCRR 1S10RR028832-01). Supported by funding from
402 the Swiss National Science Foundation PBSKP3_140135, P300P3_154633, and
403 PP00P3_163898 to C.Y.E. and C.S., and PZ00P3-185927 to A.L., the Leenaards and
404 Novartis Foundation to A.L., ETH Research Grant (ETH-30-16-2) to R.V., and NIH
405 R35GM122610 to T.K.B. Part of this research was conducted while Collin Y. Ewald
406 was an Ellison Medical Foundation/AFAR Postdoctoral Fellow.
407

Figure Legends

Figure 1

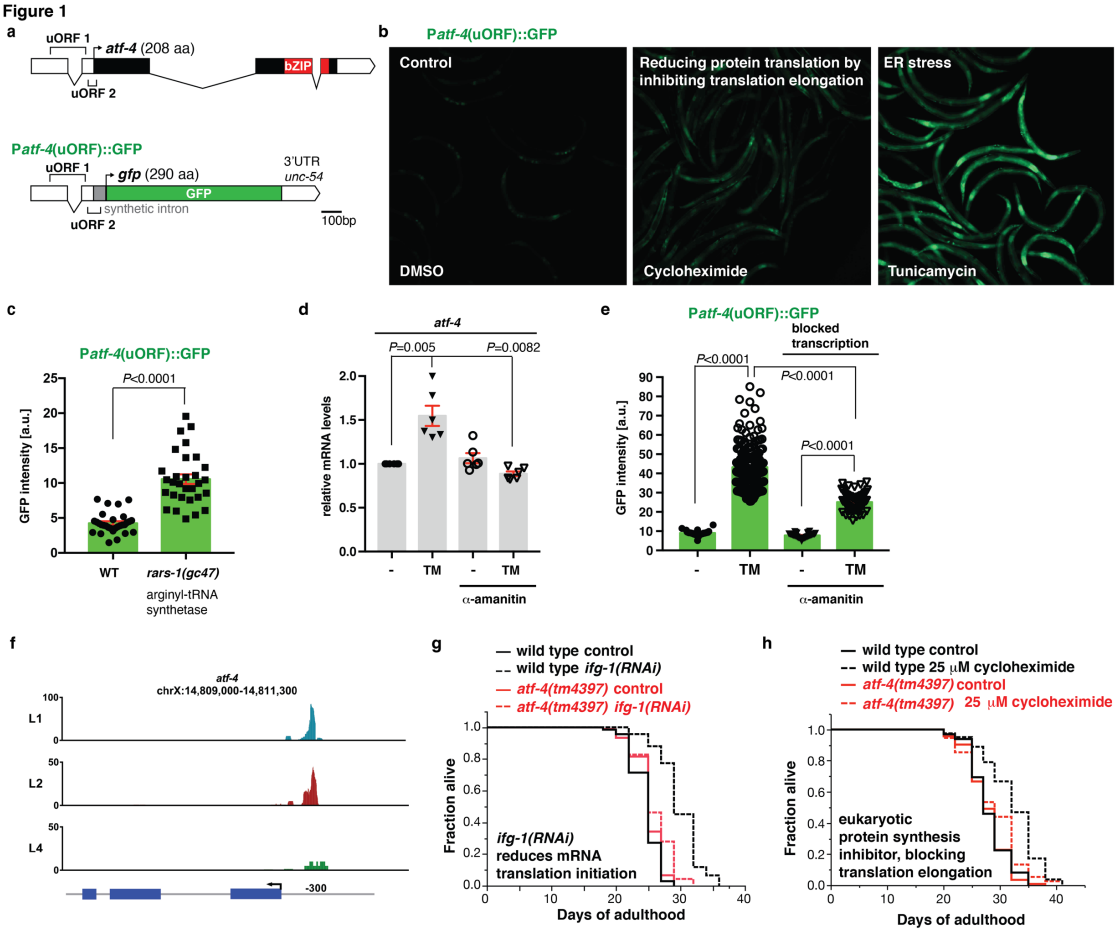

Fig. 1. Preferential translation of ATF-4 is required for longevity under conditions that reduce global protein synthesis.

a. Diagram of the *atf-4* mRNA and the P*atf-4*(uORF)::GFP reporter. For details see Extended Data Fig. 1b.

b. Reducing translation with 7.2 mM cycloheximide for 1 hour or 35 μg/ml tunicamycin for 4 hours increased expression of transgenic P*atf-4*(uORF)::GFP in L4 stage animals. Representative pictures are shown, with quantification in Extended Data Fig. 1c.

c. Nonsense mutation in the arginyl-tRNA synthetase *rars-1(gc47)* increased P*atf-4*(uORF)::GFP expression compared to WT at the L4 stage. Data are represented as mean ± s.e.m. *t*-test, unpaired, two-tailed.

d. Quantification of *atf-4* mRNA in L4 stage animals after 4 hours of 35 μg/ml tunicamycin (TM) treatment either with or without one-hour pre-treatment with 0.7 μg/ml α-amanitin (RNA Pol II inhibitor). Data are represented as mean ± s.e.m. Three independent trials, measured in duplicates. *P* values are relative to WT (N2) control determined by one sample *t*-test, two-tailed, hypothetical mean of 1.

e. The elevated GFP levels of transgenic P*atf-4*(uORF)::GFP L4 stage animals after 4 hours of 35 μg/ml tunicamycin treatment was blunted by an one hour pre-treatment with 0.7 μg/ml α-amanitin. Data are represented as mean ± s.e.m. N>30, 2 independent trials, One-way ANOVA with post hoc Tukey.

f. Stage-specific ribosome occupancy profiles of endogenous *atf-4*. Using ribosomal profiling data [61], we found an enrichment of ribosome occupancy on the endogenous *atf-4* uORFs under unstressed conditions during development, when protein synthesis is high. Occupancy profiles were generated by assigning counts to *atf-4* transcript based on the number of reads.

g. Adult-specific knockdown of *ifg-1* (eukaryotic translation initiation factor eIF4G) increased the lifespan of WT but not *atf-4(tm4397)* mutants.

h. Adult-specific treatment with 25 μM eukaryotic translation elongation inhibitor cycloheximide increased the lifespan of WT, but not of *atf-4(tm4397)* mutants.

g.-h. For statistics and additional trials see (Supplementary Table 1)

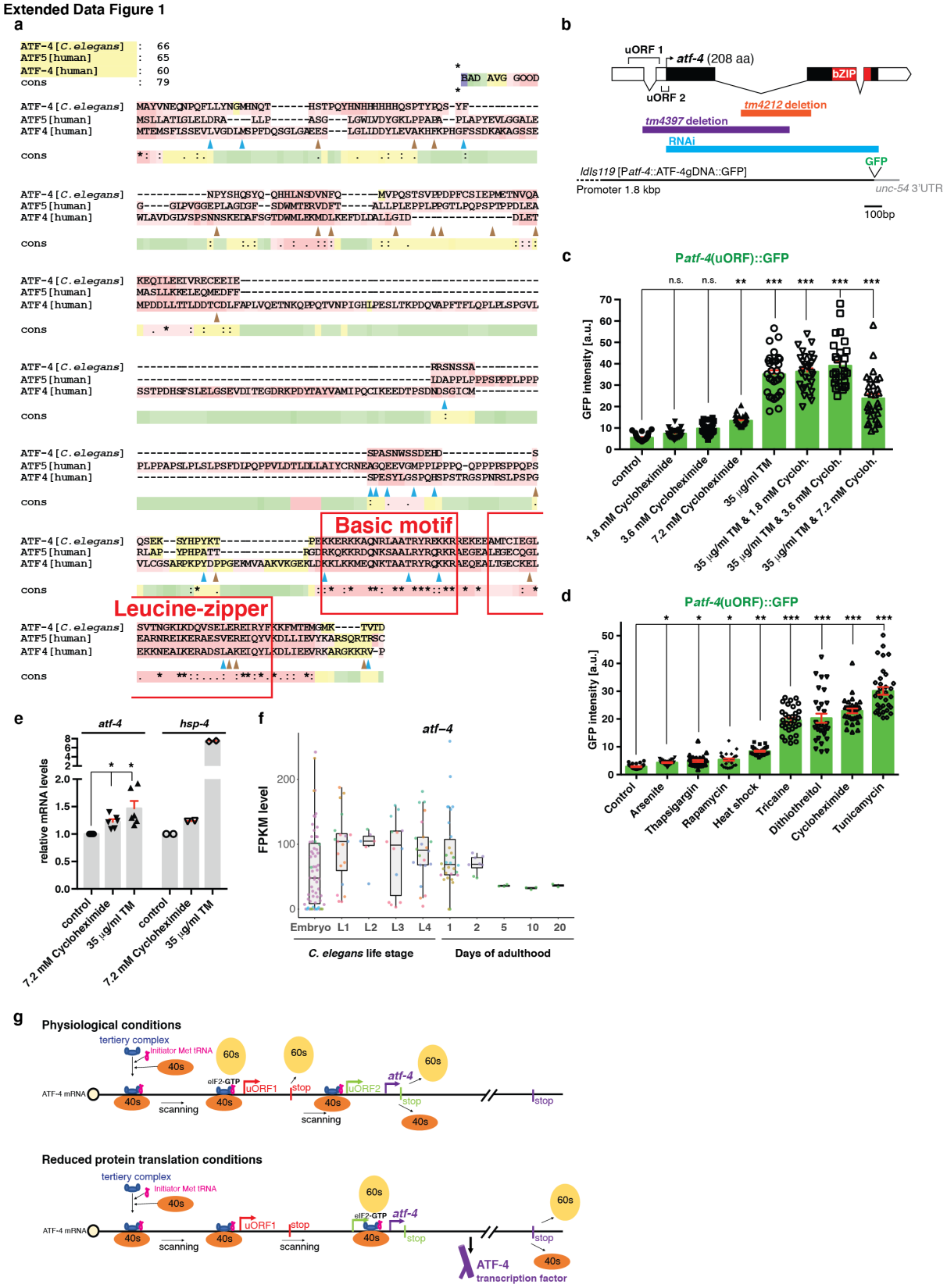

Extended Data Fig. 1. Comparison of *C. elegans atf-4* and human *ATF4*

The predicted orthologue of mammalian *ATF4* was previously named *atf-5* in *C. elegans* (www.wormbase.org. Sequence name T04C10.4, WBGene00000221). However, the basic leucine zipper (bZIP) domain of *C. elegans* ATF-5 shows higher conservation to mammalian ATF4 than ATF5 (**a, b**) and the *C. elegans atfs-1* is the functional homologue of mammalian *ATF5* [62]. Thus, we renamed *C. elegans atf-5* to *atf-4* and will refer to it as *atf-4* (activating transcription factor 4) throughout this study.

a. Alignment of *C. elegans* ATF-4 (T04C10.4, www.wormbase.org) with the human ATF4 or ATF5 amino acid sequence shows high conservation, especially in the basic and the leucine-zipper motif (red boxes). *C. elegans* ATF-4 (T04C10.4, 208 amino acids; www.wormbase.org) was aligned with Human ATF5 (282 amino acids, Q9Y2D1; www.uniprot.org) and Human ATF4 (350 amino acids, P18848; www.uniprot.org) using T-COFFEE (Version_11.00.d625267). Blue arrow heads indicate identical amino acids exclusively shared between *C. elegans* ATF-4 and human ATF4 (15 in total) and brown arrow heads indicate identical amino acids exclusively shared between *C. elegans* ATF-4 and human ATF5 (17 in total). Stars indicated identical amino acids among *C. elegans* ATF-4 and human ATF4 and ATF5 (25 in total). The basic motif of *C. elegans* ATF-4 is more similar to human ATF4 than ATF5. Stars indicate identical amino acids, single dots indicate that size or hydropathy is conserved, and double dots indicate that both size and hydropathy are conserved between the corresponding residues.

b. Diagram of *atf-4* mRNA, mutations and RNAi clone, and the *Patf-4(uORF)::GFP* transgene. The *atf-4* mRNA has an extensive 5' untranslated translated region (UTR) of 250 nucleotides containing two upstream Open Reading Frames (uORF), of which uORF1 translates into a 39 amino acids (aa) peptide and uORF2 in a 14 aa peptide.

The *tm4397* variation is an 806 base pair (bp) deletion that covers part of the uORF1, the uORF2, the translational start site and the first exon, suggesting that *tm4397* is a putative null allele. Untranslated regions (UTR) are represented as empty boxes, exons as filled boxes, basic leucine zipper domain (bZIP) in red.

c. Quantification of fluorescence of P*atf-4*(uORF)::GFP transgenic animals at L4 stage treated either with 1.8-7.2 mM cycloheximide for 1 hour and/or with 35 μg/ml tunicamycin for 4 hours. Note that pre-treatment of 7.2 mM cycloheximide for 1 hour and then with 35 μg/ml tunicamycin (TM) for 4 hours was toxic to the animals resulting in dead corpses with less GFP fluorescence. Data are represented as mean ± s.e.m. *P* values n.s. = not significant, **<0.001, and ***<0.0001 are relative to control treatment (DMSO). One-way ANOVA with post hoc Tukey.

d. *In-vivo* P*atf-4*(uORF)::GFP reporter responses upon various drug treatments or interventions that reduce mRNA translation. Transgenic P*atf-4*(uORF)::GFP L4 stage animals were treated either with 20 mM arsenite for 30 min, or 200 mM thapsigargin for 4 hours, or 100 μM rapamycin for overnight, or 30 min heat shock at 35°C, or 2% tricaine for 1 hour, or 10 mM dithiothreitol for 4 hours, or 10 mM cycloheximide for 1 hour, or 35 μg/ml tunicamycin. Data are represented as mean ± s.e.m. *P* values *<0.05, **<0.001, and ***<0.0001 are relative to control treatment. One-way ANOVA with post hoc Tukey.

e. Quantification of *atf-4* mRNA levels after cycloheximide and TM treatment of L4 stage animals. Three independent trials, measured in duplicates. In one trial, *hsp-4* mRNA was assessed as a positive control for ER stress. Data are represented as mean ± s.e.m. *P* values *<0.05 relative to control determined by one-sample *t*-test, two-tailed, a hypothetical mean of 1.

f. Expression levels of *atf-4* mRNA plotted as Fragments Per Kilobase of transcript per Million mapped reads (FPKM) during development and ageing. The *atf-4* mRNA expression levels of untreated WT *C. elegans* were retrieved using the RNAseq FPKM Gene Search tool (www.wormbase.org). The boxplots represent the overall expression pattern and the colour of the individual dots refer to the 32 individual studies used.

g. Working model for *atf-4* preferential translation. Similar to mammalian ATF4, the *C. elegans* ATF-4 also has two uORFs. After translating the first uORF, the small ribosomal subunit will continue scanning along the ATF4 mRNA. Under non-stressed condition, *i.e.*, when high amounts of the eIF2-GFP bound Met-tRNA$_i^{Met}$ are available, the small ribosomal subunit will readily acquire the eIF2 ternary complex, and the large ribosomal subunit will associate to translate the second uORF. The second uORF might be inhibitory similar to mammalian ATF4 and would inhibit the translation of the *atf-4* coding region and the ribosome will disassociate from the *atf-4* mRNA after translating the second uORF. However, under stress or reduced translational conditions, *i.e.,* low amounts of the eIF2-GFP bound Met-tRNA$_i^{Met}$ availability, the association of the large to the small ribosomal subunit is delayed, whereby the inhibitory second uORF is skipped and the re-initiation complex starts to translate the ATF-4 coding region similar as observed with mammalian ATF4. Phosphorylation of eIF2α subunit inhibits the guanine nucleotide exchange factor eIF2B, which lowers the exchange of the eIF2-GDP to eIF2-GTP and thereby lowers global mRNA translation initiation.

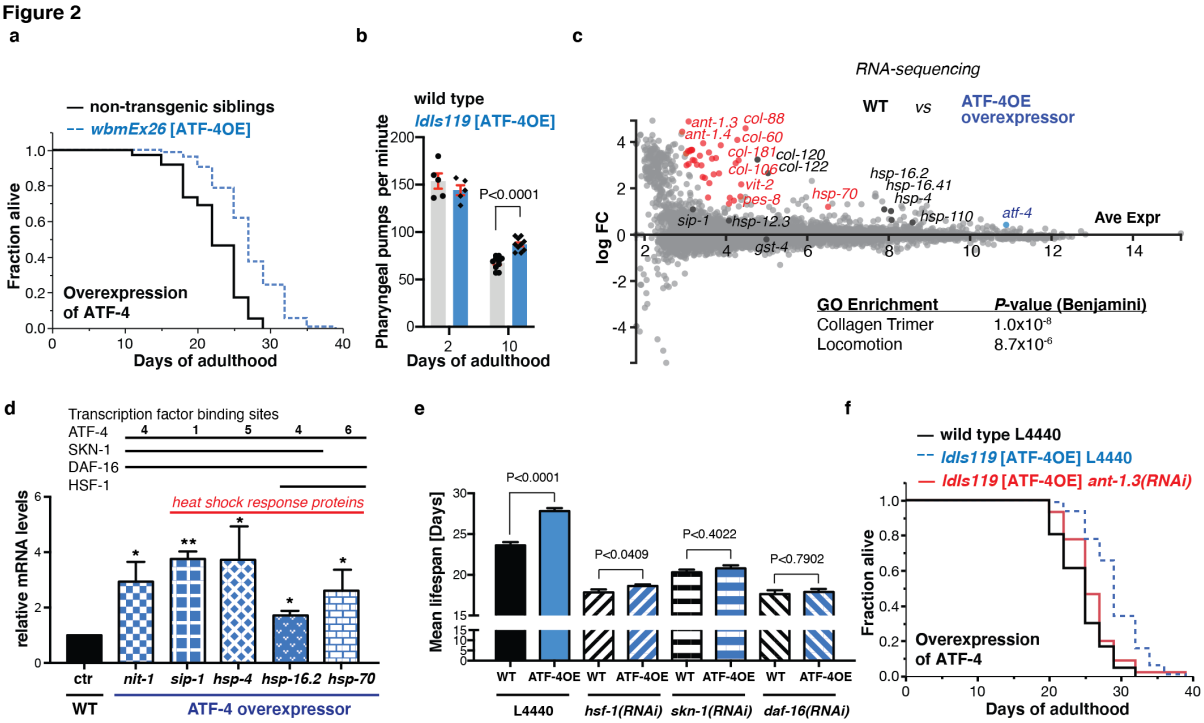

Figure 2. ATF-4 overexpression is sufficient to increase lifespan.

a. Transgenic animals (*wbmEx26* [P*atf-4*::ATF-4(gDNA)::GFP]) that overexpress ATF-4 (ATF-4oe) live longer compared to their non-transgenic siblings.

b. Pharyngeal pumping rate is similar at day 2 of adulthood between ATF-4 overexpressor (*ldIs119* [P*atf-4*::ATF-4(gDNA)::GFP]) and wild type, but higher in ATF-4 overexpressor at day 10 of adulthood, suggesting an improved healthspan. For the complete time-course of pharyngeal pumping rate during ageing, see Supplementary Table 2. *P* value determined with unpaired two-tailed *t*-test.

c. MA (log ratio and mean average)-plot of RNA sequencing analysis comparing *ldIs119* ATF-4 overexpressor to abs log FC relative to wild type. In red, highlighted genes with FDR < 0.1 and log FC > 1 compared to wild type. In black, genes with FDR > 0.1. Details in Supplementary Table 3.

d. Validation by qRT-PCR of differentially expressed *ldIs119* ATF-4 overexpressing genes using two new independent biological samples (each over 200 *C. elegans*).

529 Data are represented as mean ± s.e.m. *P* values *<0.05 and **<0.001 relative to wild
530 type determined by one sample *t*-test, two-tailed, hypothetical mean of 1. The number
531 of ATF4 binding sequences (-TGATG-) is indicated (Supplementary Table 4). The
532 DAF-16 and SKN-1 transcription factor binding sites are based on chromatin
533 immunoprecipitation ChIP data from www.modencode.org (Supplementary Table 5).
534 **e.** The longevity upon ATF-4 overexpression (*ldIs119*) on control empty vector RNAi
535 (L4440) is abolished when treated with *hsf-1(RNAi), skn-1(RNAi), or daf-16(RNAi)*.
536 Data are represented as lifespan means +/- s.e.m.
537 **f.** Mitochondrial ATP translocase *ant-1.3* is required for *ldIs119* ATF-4oe-mediated
538 longevity.
539 (**a, e, f**) For statistical details and additional lifespan trials, see Supplementary Table
540 1.
541

Extended Data Figure 2

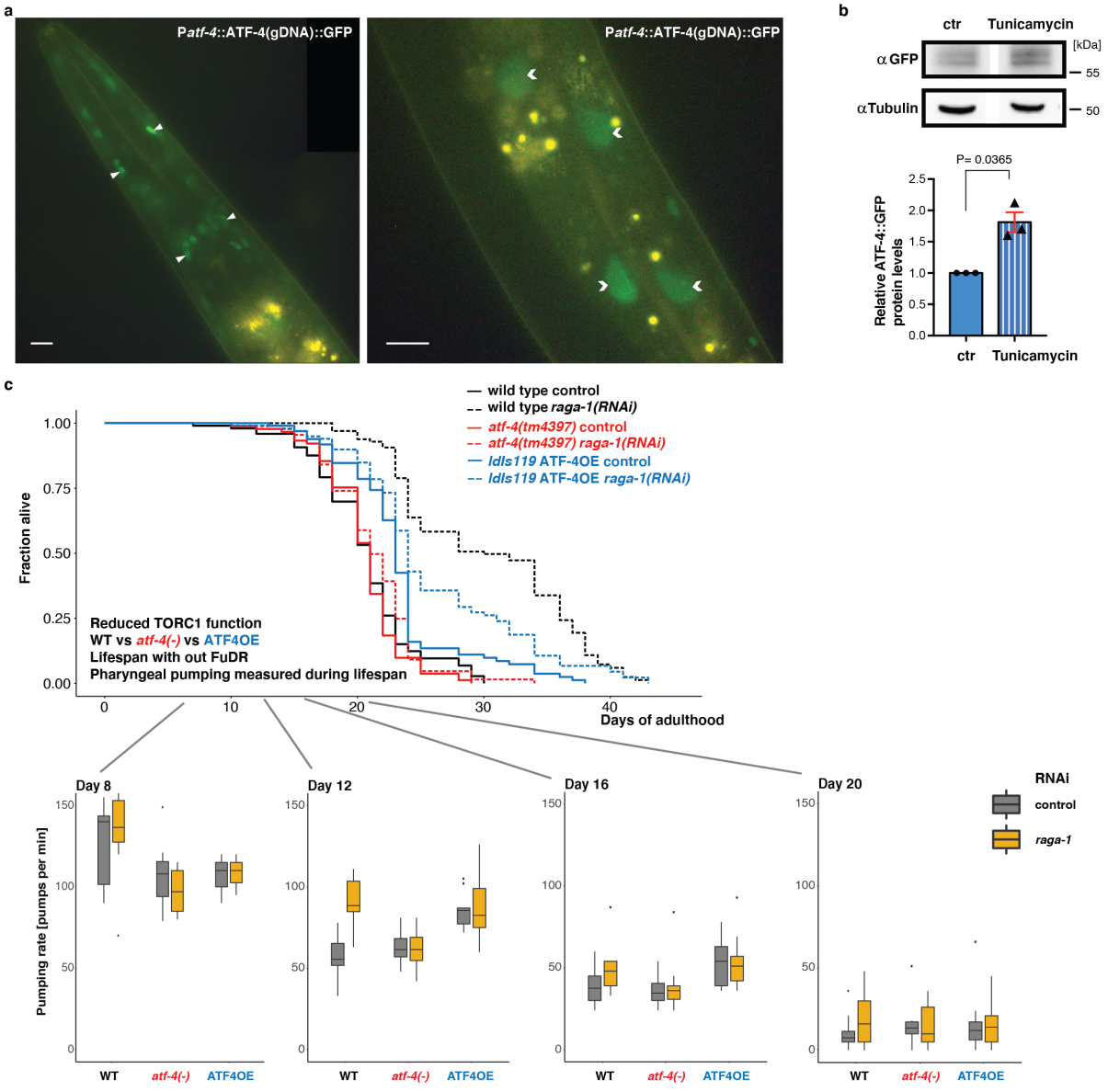

Extended Data Figure 2. Overexpression of ATF-4 increases healthspan

a. Head (left) and mid-body (right) region shown. ATF-4::GFP (*ldIs119*) is displayed in aquamarine and found predominantly in nuclei (nuclei of head neurons or glia indicated by arrowheads, intestinal nuclei indicated by chevrons). Yellow puncta are autofluorescent gut granules. 100 x magnification. Scale bar = 10 μm.

b. Western blot showing ATF-4::GFP levels and corresponding densitometry of day-1-adult transgenic *ldIs119* [P*atf-4*::ATF-4(gDNA)::GFP] either treated with control (ctr) solvent (DMSO) or 35 μg/mL tunicamycin for 6 hours. Corresponding and additional

551 western blots are shown in Supplementary Data File 1. Data are represented as mean
552 ± s.e.m. *P*-value is relative to ctr determined by one-sample *t*-test, two-tailed, a
553 hypothetical mean of 1.
554 **c**. Pharyngeal pumping measurements during the lifespan comparing wild type (N2),
555 *atf-4(tm4397)* mutants, and ATF-4 overexpression (*ldIs119*) either treated with empty
556 vector control RNAi (L4440) or *raga-1(RNAi)* on culturing plates that do not contain
557 FuDR. See Supplementary Table 2 for raw data on pharyngeal pumping rates.
558

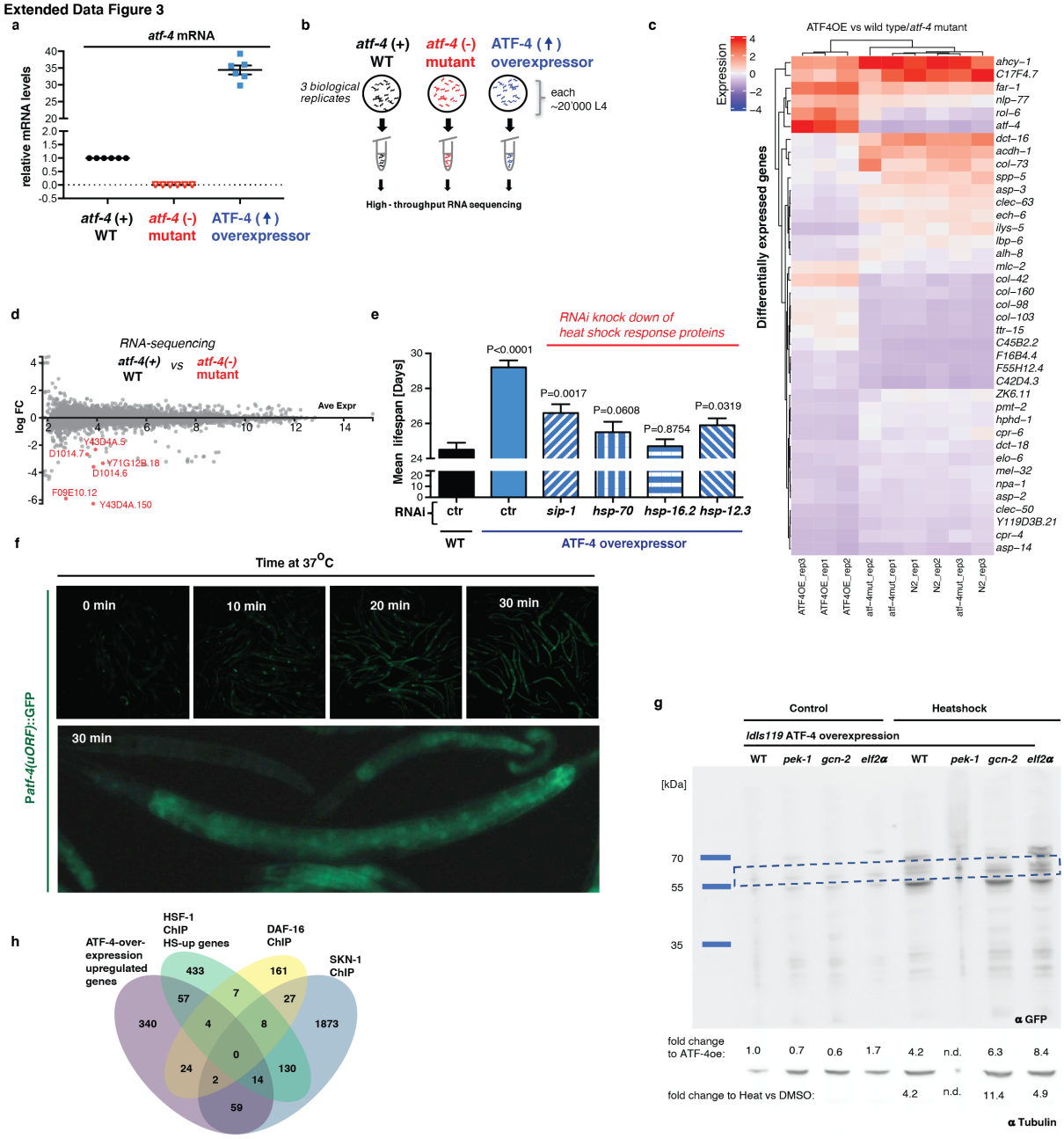

559

560 **Extended Data Figure 3. RNA-sequencing comparison of ATF-4 overexpression**

561 **vs wild type.**

562 **a.** Comparing *atf-4* mRNA expression levels of *atf-4(tm4397)* mutants (*atf-4* (-) mutant)

563 and ATF-4 overexpressor (*ldIs119* [P*atf-4*::ATF-4(gDNA)::GFP]) relative to wild type

564 (*atf-4*(+) WT) by qRT-PCR. The *atf-4(tm4397)* mutants showed zero *atf-4* mRNA

565 expression levels, reconfirming a putative null allele. These samples were used for

566 RNA sequencing. Three independent biological replicates of about 20'000 L4 *C.*

elegans (see Materials and Methods). *P* values for both *atf-4(tm4397)* or ATF-4 overexpressor (*ldIs119*) are <0.0001 relative to wild type determined by one-sample *t*-test, two-tailed, a hypothetical mean of 1.

b. Schematic representation of sample collection for RNA sequencing. See Materials and methods for details. Three biological replicates comparing wild type (*atf-4*(+) WT), *atf-4(tm4397)* mutants (*atf-4* (-) mutant), and ATF-4 overexpressor (*ldIs119* [P*atf-4*::ATF-4(gDNA)::GFP]). More than 20'000 L4 *C. elegans* were collected per strain and biological replicate.

c. Hierarchical clustering heatmap of the genes that are most differentially regulated in either direction when comparing ATF-4 overexpressors (ATF-4OE, *ldIs119* [P*atf-4*::ATF-4(gDNA)::GFP]) to wild type (*atf-4*(+) WT) and *atf-4(tm4397)* mutants (*atf-4* (-) mutant). As expected, *atf-4* is in the top gene set, since comparing ATF-4 overexpression and *atf-4* deletion mutant to wild type. The collagen *rol-6* is the co-injection marker for the transgenic *ldIs119*. Independent biological replicates are indicated as "rep#". For details and raw data see Supplementary Table 3.

d. MA (log ratio and mean average)-plot of RNA sequencing analysis comparing *atf-4(tm4397)* mutants (*atf-4* (-) mutant) to absolute log fold-change (FC) relative to wild type (*atf-4* (+) WT). In red, highlighted genes with a false discovery rate (FDR) < 0.1 and abs log FC > 1 to wild type. Details in Supplementary Table 3.

e. The longevity upon ATF-4 overexpression (*ldIs119*) on control empty vector RNAi (L4440) is blunted by knockdown with *sip-1(RNAi), hsp-70(RNAi), hsp-16.2(RNAi),* or *hsp-12.3(RNAi)*. Data are represented as lifespan means +/- s.e.m. P values are relative to wild type on empty vector RNAi (L4440). For statistical details see Supplementary Table 1.

591 **f.** P*atf-4(uORF)*::GFP transgenic *C. elegans* were placed at 37°C for 0-30 min and the
592 GFP induction was scored. Bottom panel, 30 min at 37°C, higher magnification. Shown
593 L4 P*atf-4(uORF)*::GFP transgenic *C. elegans*, anterior to the right, ventral side down.
594 **g**. Preferential translation of ATF-4 upon heat shock**.** Transgenic *ldIs119* [ATF-4::GFP]
595 at L4 stage were heat shocked at 37°C for 1 hour, let recover for 4 hours at 25°C or
596 were kept for 5 hours at 25°C as control, and then harvested for western blotting using
597 GFP antibodies to determine ATF-4::GFP protein levels. Equal amounts of samples
598 were run in parallel on a separate blot to assess tubulin levels.
599 **h.** Venn diagram showing the overlap of *ldIs119* ATF-4oe overexpression-upregulated
600 genes with genes that were bound directly by SKN-1, DAF-16, and HSF-1 in chromatin
601 immunoprecipitation ChIP studies. For details and references see Supplementary
602 Table 5.
603

Figure 3

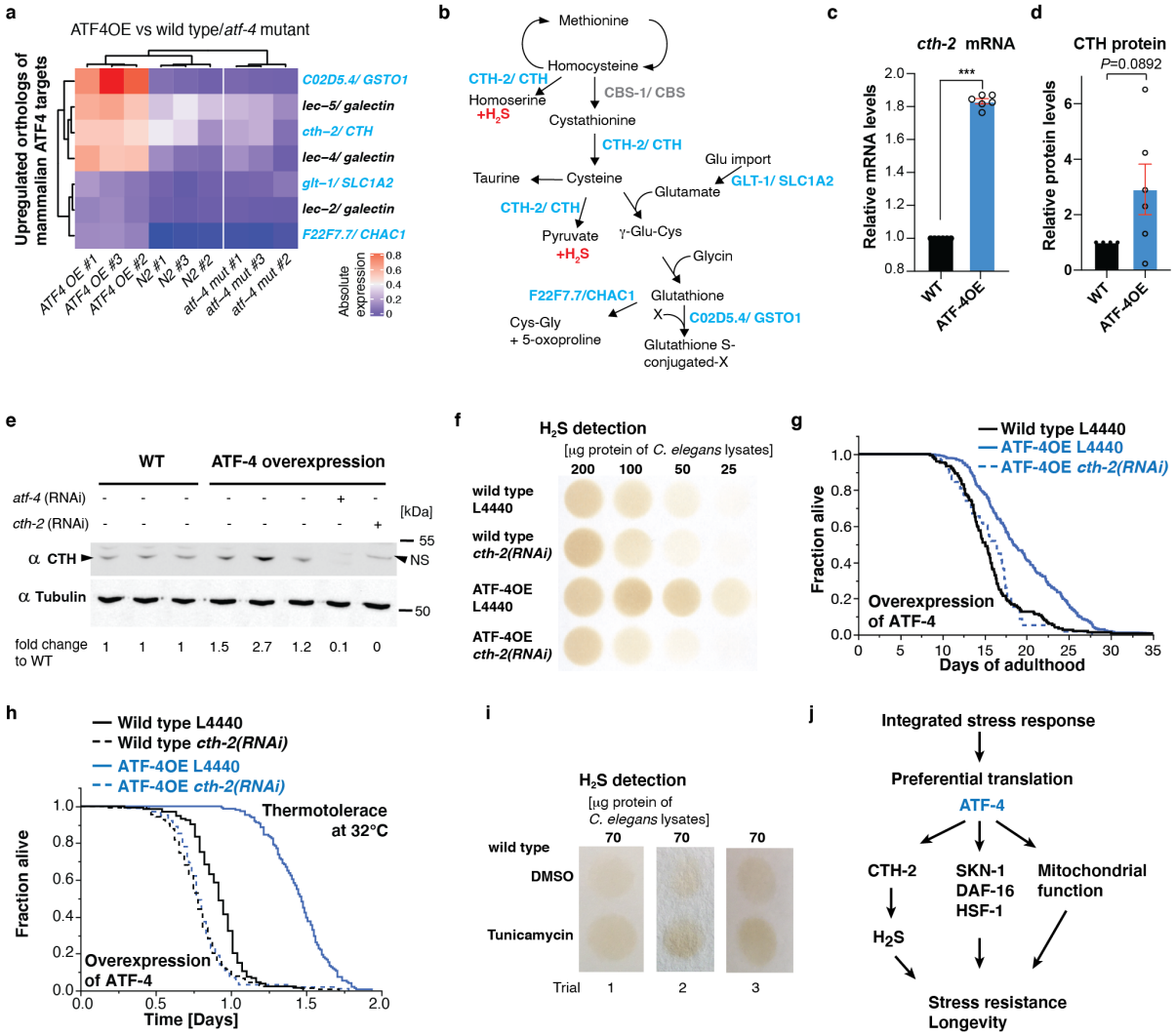

Figure 3. ATF-4 overexpression increases hydrogen sulfide levels via cystathionine gamma-lyase required for longevity and stress resistance.

a. Heatmap of *ldIs119* ATF-4 overexpressor vs WT and *atf-4(tm4397)* showing orthologs of genes that are directly regulated by mammalian ATF4 (Details are in Materials and Methods, Supplementary Table 4). Absolute levels of expression were compared. Genes indicated in light blue are predicted to be involved in the transsulfuration pathway shown in Fig. 3b.

b. Schematic of the transsulfuration pathway. Genes in light blue were found to be upregulated by ATF-4 overexpression (Fig. 3a, Supplementary Table 4).

c. ATF-4 overexpressor (*ldIs119*) showed higher *cth-2* mRNA levels compared to wild type (WT) by qRT-PCR. Three independent biological samples in duplicates (each over 200 L4 *C. elegans*). Data are represented as mean ± s.e.m. *P* values *<0.05 and ***<0.0001 relative to wild type determined by one-sample *t*-test, two-tailed, a hypothetical mean of 1.

d. Quantification of CTH protein levels of ATF-4 overexpressor (*ldIs119*) compared to wild type (WT). Six independent biological trials probed in three western blots. Full blots are shown in Supplementary Data File 2.

e. Western blot probing CTH levels showed higher CTH levels when ATF-4 is overexpressed (*ldIs119*), but was abolished by knockdown of *atf-4* or *cth-2*. Biological repeats and full blots shown in Supplementary Data File 2. NS = non-specific band.

f. Hydrogen sulfide production capacity assay from whole *C. elegans* lysates showed that *ldIs119* ATF-4 overexpressor (ATF-4oe) produced more H_2S compared to wild type (WT) and these higher H_2S levels were abolished when *cth-2* was knocked down. Additional biological trials are shown in Extended Data Fig. 4a-e.

g. The heat stress resistance mediated by *ldIs119* ATF-4 overexpressor (ATF-4oe) was suppressed by knockdown of *cth-2*. For statistical details and additional trials see Supplementary Table 7.

h. The longevity mediated by *ldIs119* ATF-4 overexpressor (ATF-4oe) was suppressed by knockdown of *cth-2*. For statistical details and additional lifespan trials see Supplementary Table 1.

i. Tunicamycin treatment increased hydrogen sulfide production. Wild type L4 worms were treated with DMSO as a control or 35 μg/ml tunicamycin for 4 hours. Three independent biological trials are shown.

638 **j.** Model of ATF-4 mediated downstream programs.

639

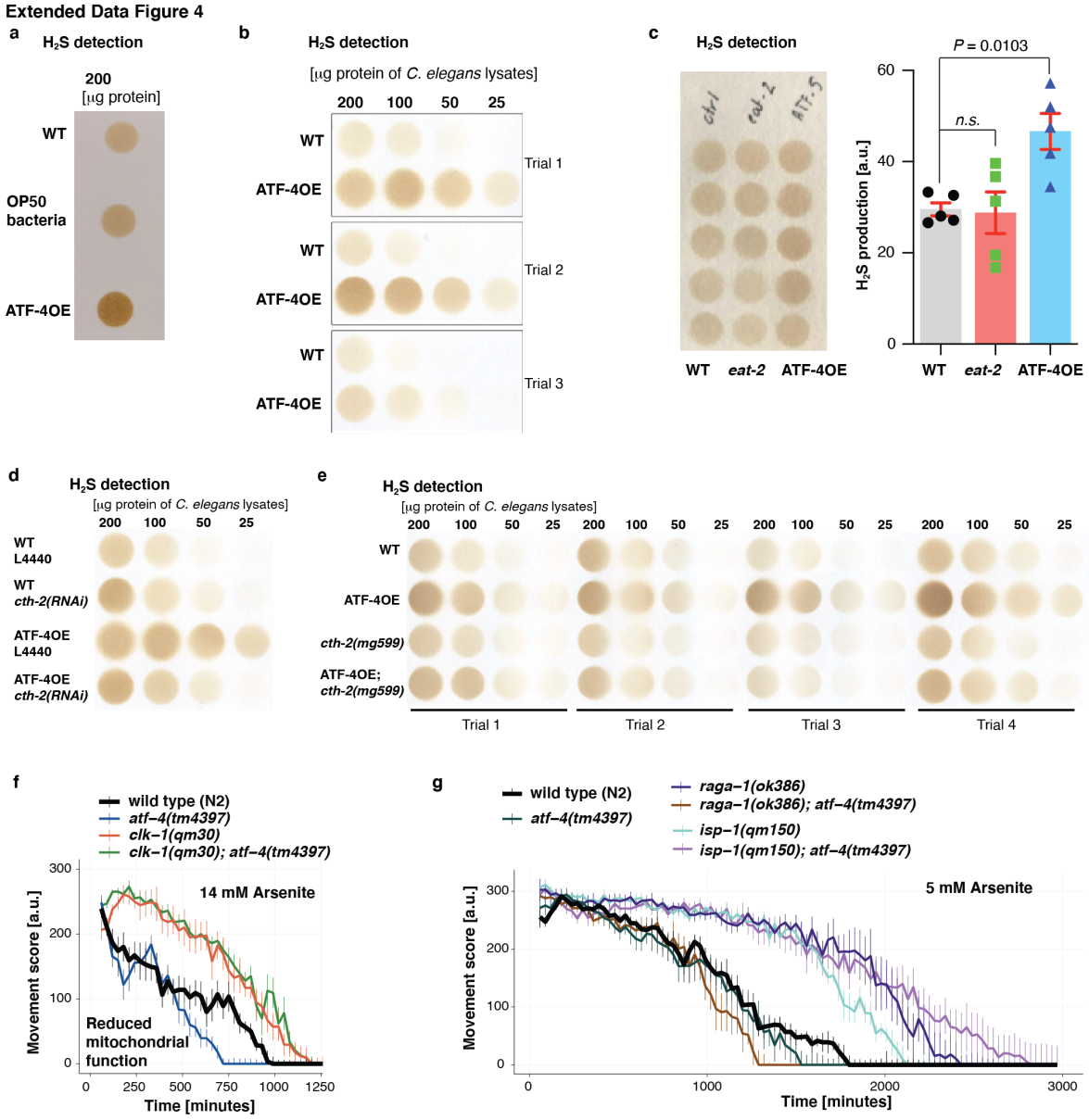

Extended Data Figure 4. ATF-4 overexpression increases hydrogen sulfide levels via cystathionine gamma-lyase.

a. Hydrogen sulfide production capacity assay. 200 *µ*g of total protein lysate either from wild-type *C. elegans* (WT), food source OP50 *E. coli* bacteria, or *ldIs119* ATF-4 overexpressor transgenic *C. elegans* (ATF-4oe) were loaded. Since OP50 *E. coli* bacteria protein lysates have the capacity to produce H_2S, we washed *C. elegans* at least three times or until no bacteria visible in the supernatant.

b. Hydrogen sulfide production capacity assay from whole *C. elegans* lysates showed that *ldIs119* ATF-4 overexpressor (ATF-4oe) produced more H_2S compared to wild type (WT) in three independent biological trials.

c. Hydrogen sulfide production capacity of 2 *μ*g/ml lysates from wild type (WT), *eat-2(ad1116)* mutants, and *ldIs119* ATF-4 overexpressor transgenic *C. elegans* (ATF-4oe). H_2S levels were quantified as the amount of lead sulfide captured on the paper, measured by the integrated density of each well area. Data are represented as mean $\pm$ s.e.m. *P*-values were determined with One-way ANOVA post hoc Tukey.

d. Hydrogen sulfide production capacity assay from whole *C. elegans* lysates showed that *ldIs119* ATF-4 overexpressor (ATF-4OE) produced more H_2S compared to wild type (WT) and these higher H_2S levels are abolished when *cth-2* was knocked down in a second biological trial (as in Fig. 3f showing first biological trial).

e. Hydrogen sulfide production capacity assay from whole *C. elegans* lysates. ATF-4OE (*ldIs119*) showed higher H_2S compared to wild type (WT) and these higher H_2S levels are abolished in *cth-2(mg599)* mutant background.

f. Loss of *atf-4* did not suppress the oxidative stress resistance in 14 mM arsenite of reduced mitochondrial function mutant *clk-1(qm30)*.

g. Loss of *atf-4* did not suppress the oxidative stress resistance in 5 mM arsenite of reduced mitochondrial function mutant *isp-1(qm150),* but of reduced TORC1 mutant *raga-1(ok386)*.

For **f-g.** For statistical details and additional trials see Supplementary Table 8.

Figure 4

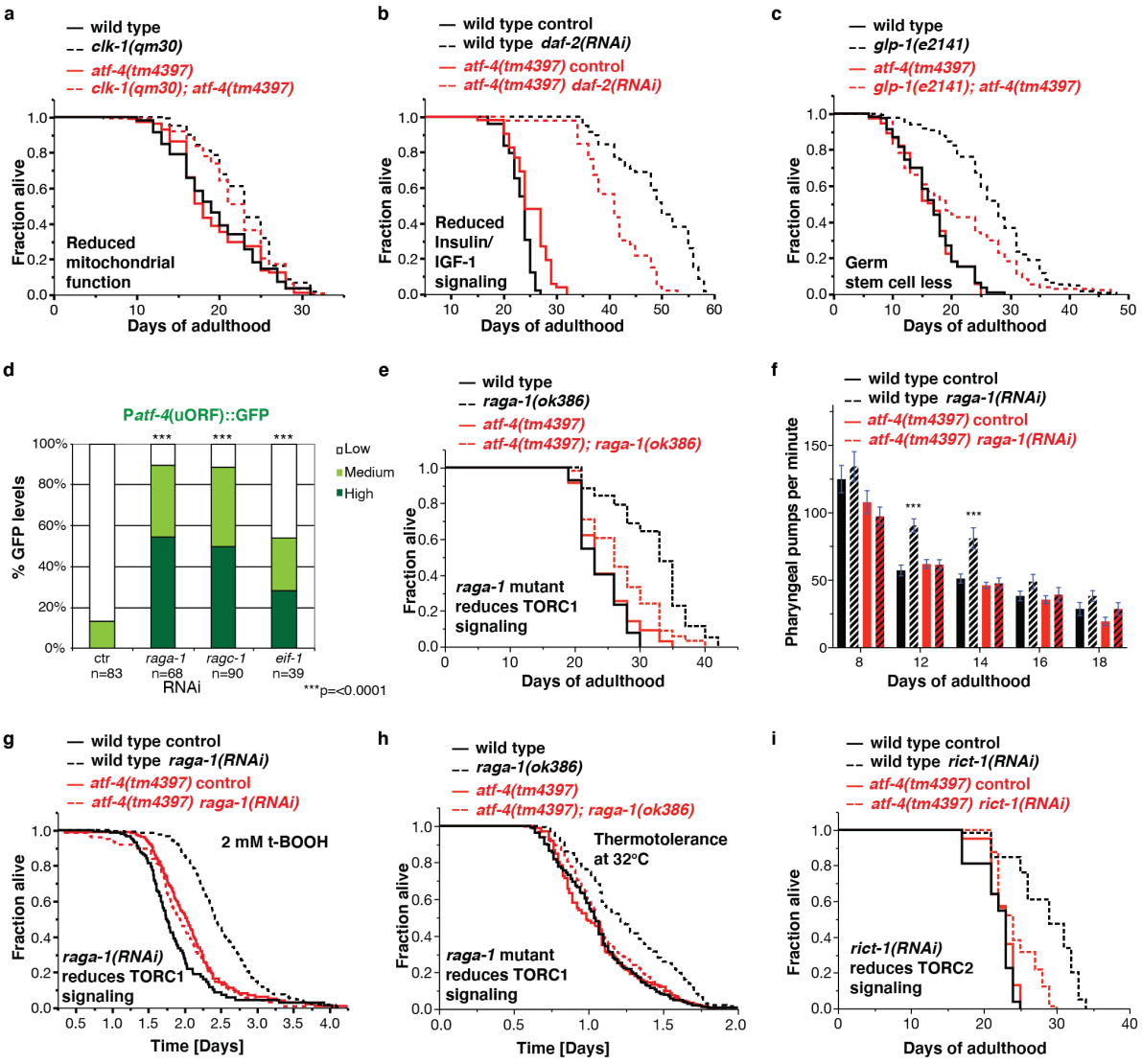

Figure 4. ATF-4 is essential for longevity from reduced mTORC1 activity

a. Loss of *atf-4* did not suppress the longevity of reduced mitochondrial function mutant *clk-1(qm30)*.

b. Extending lifespan reducing Insulin/IGF-1 signalling by *daf-2(RNAi)* treatment starting from adulthood is partially suppressed by *atf-4(tm4397)* mutation.

c. The longevity of germ cell proliferation *glp-1(e2141)* mutants was partially suppressed by *atf-4(tm4397)* mutation

d. Inhibition of TORC1 by RNAi of *raga-1*, *ragc-1* or by inhibition of translation via knockdown of eukaryotic initiation factor *eif-1* leads to preferential translation of ATF-

4 using the P*atf-4*(uORF)::GFP reporter strain. RNAi treatment was started at L4 until mounted to score GFP intensity using a microscope scope at 40x at day 3 of adulthood. Scoring described in Materials and Methods. *P* values determined by Chi^2 test. Additional trials also including TORC2 are in Supplementary Table 9.

e. Mutation in *raga-1* increases lifespan in an *atf-4*-dependent manner.

f. Reducing TORC1 signalling by adulthood specific *raga-1* RNAi improves healthspan as assessed as pharyngeal pumping rate in an *atf-4*-dependent manner. Data represented as mean $\pm$ S.E.M. *** P<0.0001 relative to wild type control of the corresponding day with One-way ANOVA with post hoc Dunnett's multiple comparisons test. Raw data in Supplementary Table 2.

g. Adult-specific knockdown of TORC1 subunit *raga-1* extends oxidative stress resistance in 2 mM t-BOOH in an *atf-4*-dependent manner. L4 animals were treated with RNAi, and stress resistance was measured at day 3 of adulthood with the automated lifespan machine. For additional trials, statistical details, and raw data, see Supplementary Table 10.

h. Heat stress resistance at 32^{o}C of TORC1 *raga-1(ok386)* mutants depends on *atf-4*. For additional trials, statistical details, and raw data, see Supplementary Table 7.

i. Adult-specific knockdown of TORC2 subunit *rict-1* extends lifespan in an *atf-4*-dependent manner.

For **a-c, e, i.** For statistical details and additional lifespan trials see Supplementary Table 1.

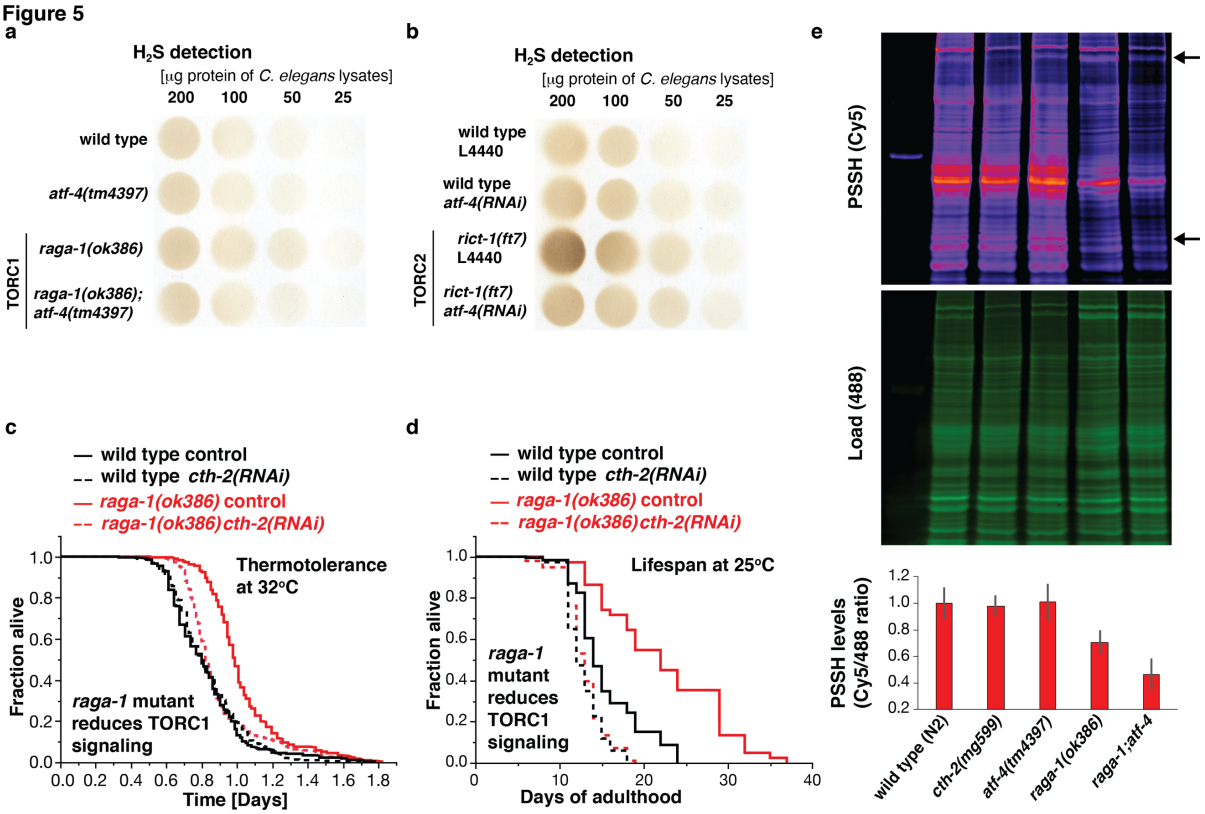

Figure 5. Longevity from mTOR inhibition upregulates H_2S and requires *cth-2*

a. Hydrogen sulfide production capacity assay from whole *C. elegans* lysates showed that TORC1 *raga-1(ok386)* mutants produced more H_2S compared to wild type or *atf-4(tm4397)* mutant in an *atf-4*-dependent manner. Two additional independent biological trials are shown in Extended Data Fig. 5f-g.

b. Hydrogen sulfide production capacity assay from whole *C. elegans* lysates showed that TORC2 *rict-1(ft7)* mutants produced more H_2S compared to wild type or *atf-4(tm4397)* mutant in an *atf-4*-dependent manner. An additional independent biological trial is shown in Extended Data Fig. 5h.

c. Heat stress resistance at 32°C of TORC1 *raga-1(ok386)* mutants depends on *cth-2*. For additional trials, statistical details, and raw data, see Supplementary Table 7.

d. Longevity of TORC1 *raga-1(ok386)* mutants depends on *cth-2*. For statistical details and additional lifespan trials see Supplementary Table 1.

716 **e.** Persulfidation levels in wild type (N2), *cth-2 (mg599)*, *atf-4 (tm4397)*, *raga-1 (ok386)*
717 and *raga-1;atf-4* mutants detected using in-gel dimedone switch method. 488 signal
718 shows the total protein load. Ratio of Cy5/488 signals was used for the quantification.
719 ~15000 worms were lysed per protein lane. n = 3. Arrows indicate proteins that are
720 different persulfidated among genotypes.
721

Extended Data Figure 5

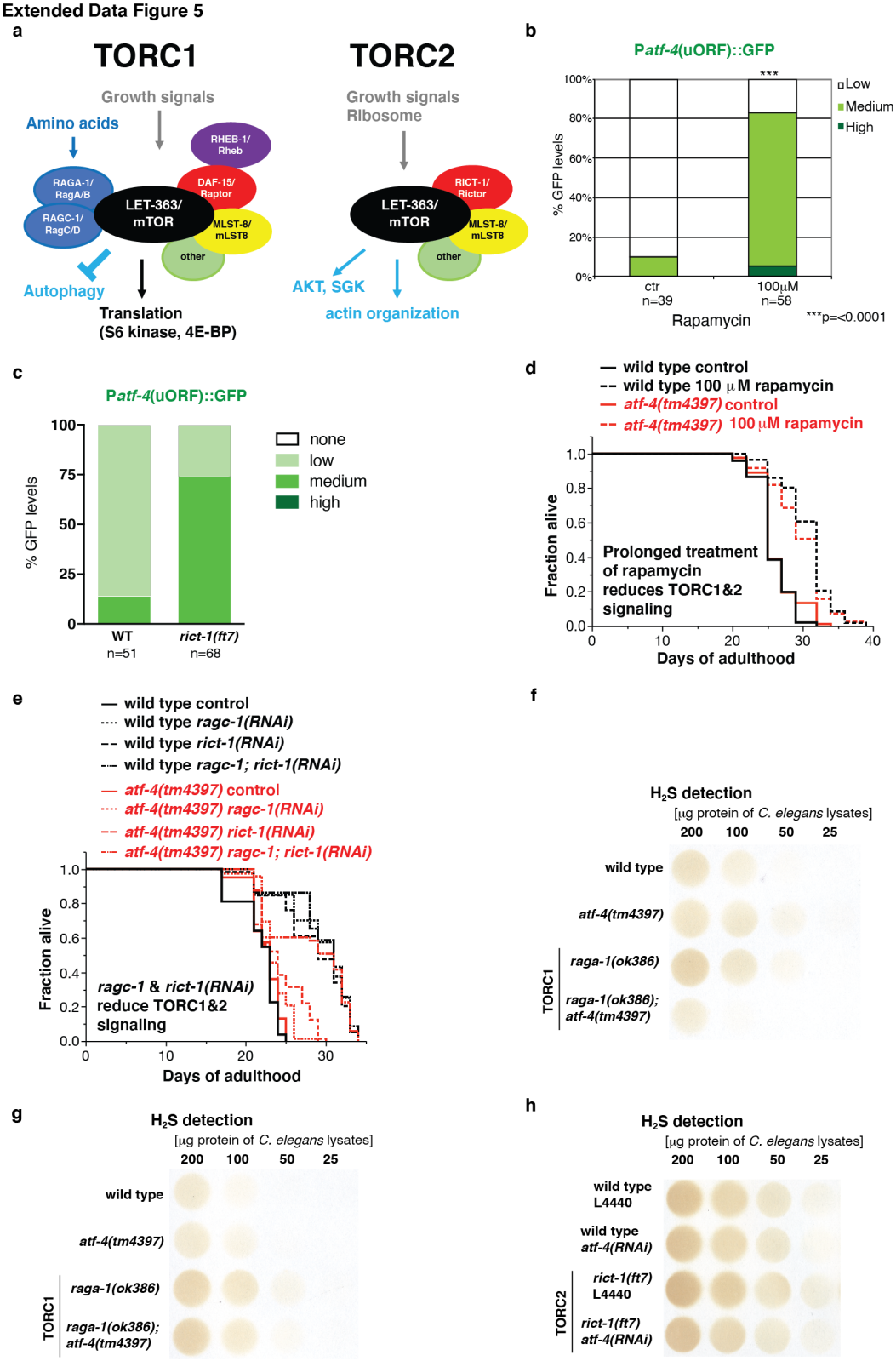

Extended Data Figure 5. Preferential *atf-4* translation and H_2S signalling upon reduced TOR signalling.

a. Schematic representation of the two TOR complexes (TORC1 and TORC2) and function adapted from [14].

b. Rapamycin treatment leads to preferential translation of ATF-4 using the P*atf-4*(uORF)::GFP reporter strain. RNAi treatment was started at L4 until mounted to score GFP intensity using a microscope scope at 40x at day 3 of adulthood. Scoring described in Materials and Methods. *P* values determined by Chi^2 test. Additional trials in Supplementary Table 9.

c. TORC2 mutants *rict-1(ft7)* showed preferential translation of ATF-4 using the P*atf-4*(uORF)::GFP reporter strain. Additional trials in Supplementary Table 9.

d. Prolonged rapamycin treatment during adulthood extends lifespan independent of *atf-4* (Supplementary Table 1).

e. Adult-specific knockdown of either TORC1 subunit *ragc-1* or TORC2 subunit *rict-1* requires *atf-4* to increase lifespan, whereas double knockdown of both complexes increases lifespan independent of *atf-4*. Complementary to this, longevity through prolonged rapamycin treatment, which might lead to simultaneous inhibition of TORC1 and TORC2, is independent of *atf-4* (Supplementary Table 1).

f-g. Hydrogen sulfide production capacity assay from whole *C. elegans* lysates showed that TORC1 *raga-1(ok386)* mutants produced more H_2S compared to wild type or *atf-4(tm4397)* mutant in an *atf-4*-dependent manner. An additional independent biological trial is shown in Fig. 5a.

h. Hydrogen sulfide production capacity assay from whole *C. elegans* lysates showed that TORC2 *rict-1(ft7)* mutants produced more H_2S compared to wild type or *atf-4(tm4397)* mutant in an *atf-4*-dependent manner. An additional independent biological trial is shown in Fig. 5b.

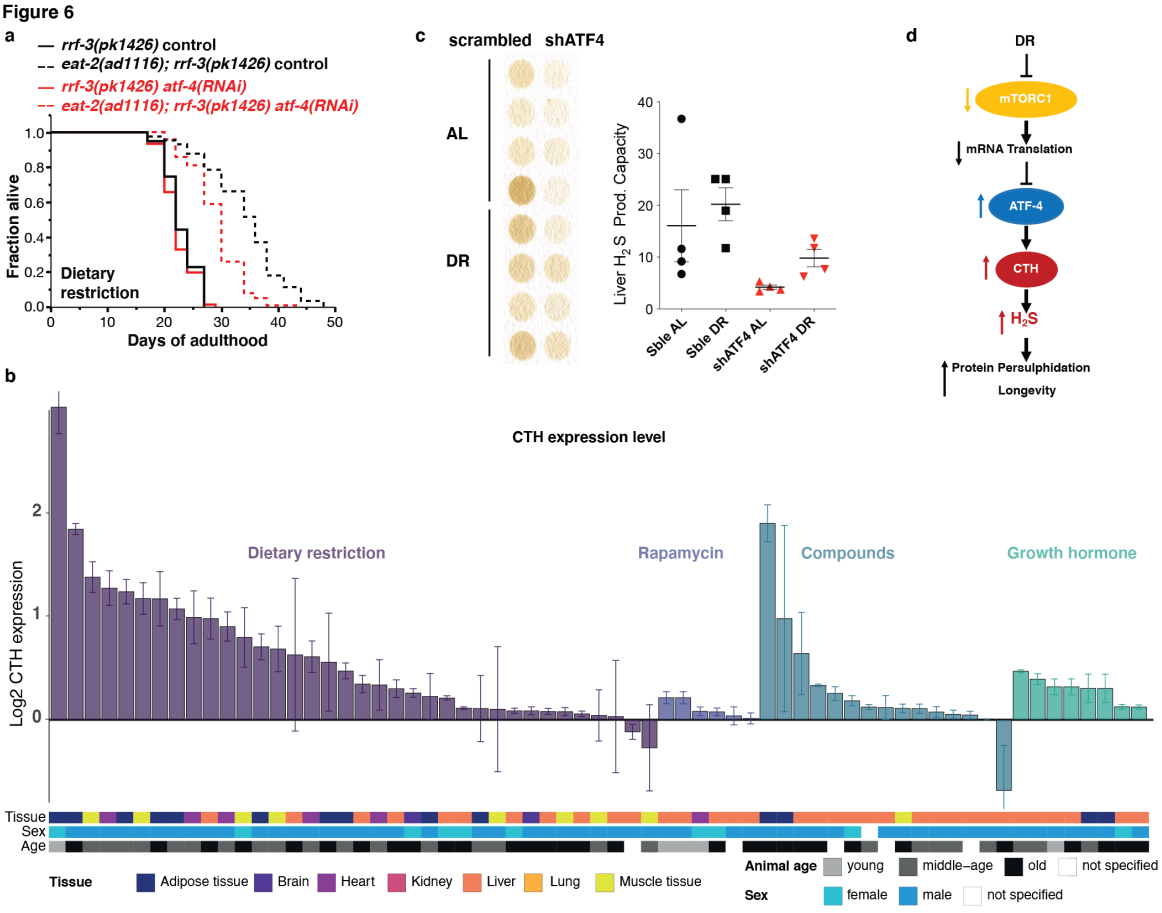

Figure 6. Dietary restriction requires ATF4 for H_2S induction in mice and longevity in *C. elegans*.

a. Knockdown of *atf-4* by RNAi partially suppresses the longevity of dietary restriction model *eat-2*. We used an RNAi-sensitized background (*rrf-3(pk1426)*; Supplementary Table 1).

b. CTH mRNA expression levels in long-lived over control mice analysed from publicly available expression datasets (Supplementary Table 11). Data is grouped and colored by interventions and represented as mean ± s.e.m. The meta data of the samples is summarised by coloured tiles indicating first the tissue of origin then the sex and then the age group of the mice in each experiment. Animals sacrificed before 16 weeks of age were classified as “young”, between 16 to 32 weeks as “middle-aged” and animals

761 above 32 weeks as “old”. In case no meta information could be found, it was labelled
762 as “not specified”.
763 **c.** Blot of hydrogen sulfide production assay of dietary restricted livers was higher than
764 in livers of ad libitum feed mice, which was suppressed by knockdown of *ATF4* as
765 quantified in the right panel.
766 **d.** ATF-4 mediates inducible H_2S production and longevity from DR and mTORC1
767 inhibition.
768

Data Source File showing full western blots and independent repeats.

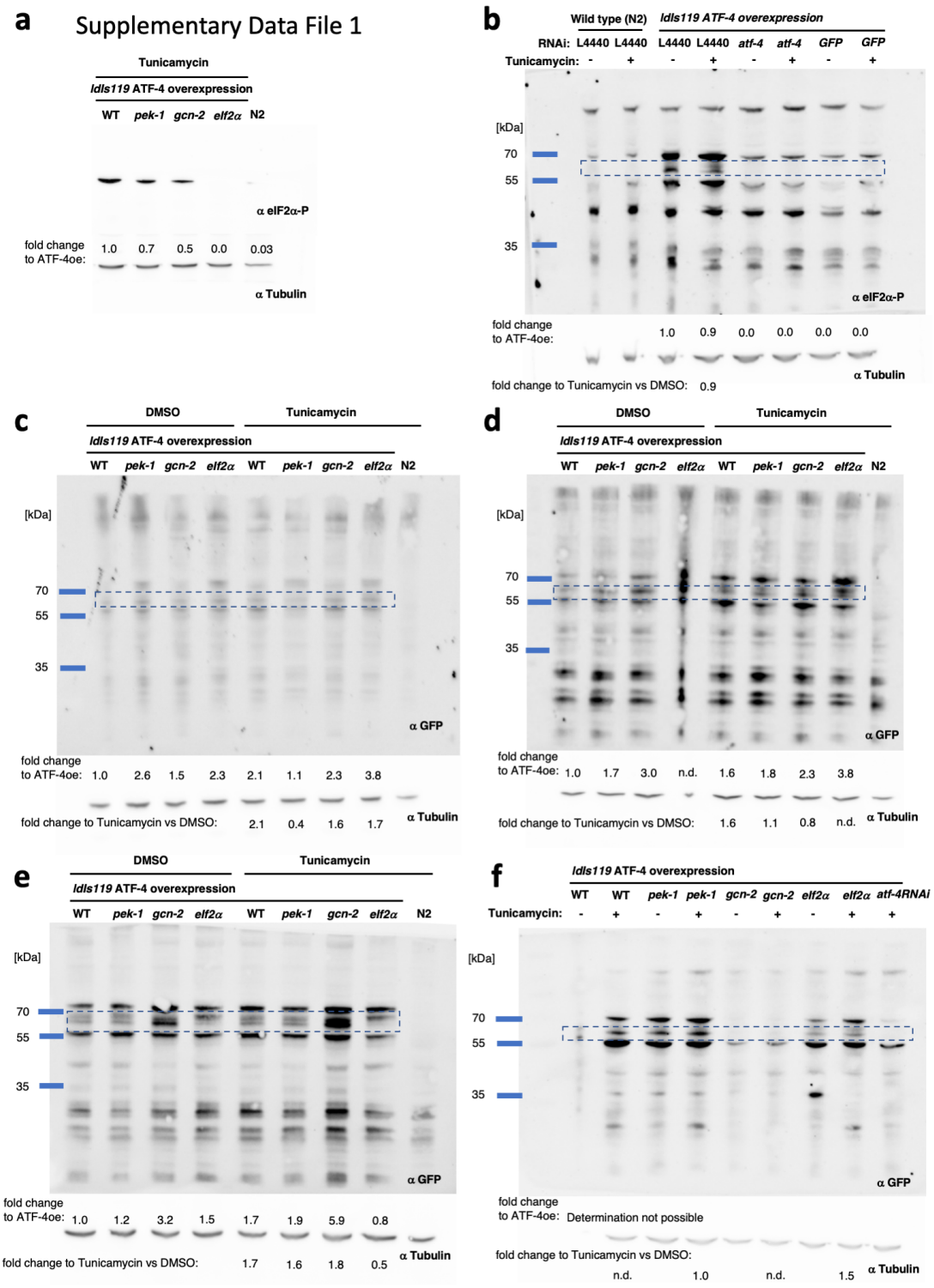

771 **Supplementary Data File 1. ATF-4 protein levels in gain-of-function transgenic**
772 ***Idls119* [ATF-4::GFP] overexpressing animals are mildly induced with**
773 **tunicamycin treatment.**

774 The predicted size *C. elegans* ATF-4 (208 amino acids; www.wormbase.org) is about
775 25 kDa and for the fusion protein of ATF-4::GFP in *Idls119* transgenic animals is about
776 55 kDa.

777 **a.** Phosphorylation of eIF2alpha was measured in *Idls119* (WT), *Idls119; pek-*
778 *1(ok275) (pek-1), Idls119; gcn-2(ok886) (gcn-2) and Idls119; eif2a(qd338) (eif2a)* after
779 treatment of tunicamycin (35 μg / ml) for six hours at 25°C.

780 **b.** GFP antibody blotted against wild type (N2) or *Idls119* [ATF-4::GFP] treated for one
781 generation with empty vector control L4440, *atf-4(RNAi),* or *gfp(RNAi)* in the presence
782 or absence of tunicamycin.

783 **c-f.** GFP antibody blotted against wild type (N2) (or N2 with *atf-4(RNAi)* in **f**), *Idls119*
784 (WT), *Idls119; pek-1(ok275) (pek-1), Idls119; gcn-2(ok886) (gcn-2),* or *Idls119;*
785 *eif2a(qd338) (eif2a)* in the presence or absence of tunicamycin.

786 For **b.-f**. Animals of their first day of adulthood were treated either with tunicamycin
787 (35 μg / ml) for six hours at 25°C or a corresponding amount of DMSO dissolved in
788 M9.

789 In all samples an antibody against Tubulin was used as control either if protein sizes
790 permitted, the membrane was cut and tubulin levels were assessed, or blot after GFP
791 antibody usage was stripped (in **b**), or equal amounts of sample was run in parallel on
792 a separate blot (**c.-f.**).

793

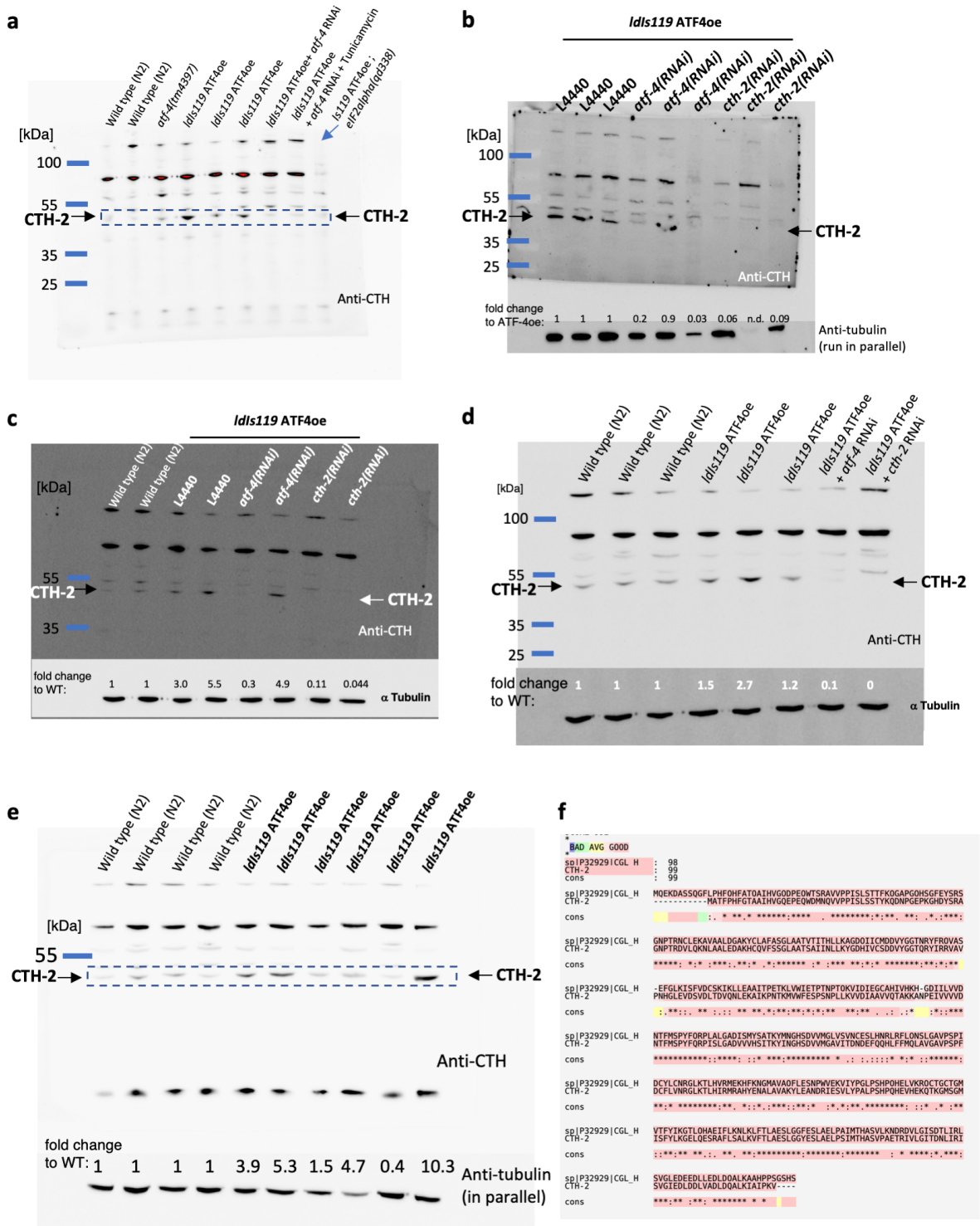

794

795 **Supplementary Data File 2. ATF-4 overexpressor showed higher cystathionine**

796 **gamma lyase CTH-2 protein levels**

The predicted size *C. elegans* CTH-2 (392 amino acids; www.wormbase.org) is about 43 kDa. The Anti-Cystathionase/CTH antibody ab151769 is a recombinant fragment corresponding to Human Cystathionase/CTH amino acids 194-405. This part is well conserved (**f**)

a-e. CTH antibody blotted against wild type (N2) or *ldIs119* [ATF-4::GFP] treated for one generation with empty vector control L4440, *atf-4(RNAi),* or *cth-2(RNAi).*

f. Alignment of *C. elegans* CTH-2 (ZK1127.10; 392 amino acids; www.wormbase.org) with human CTH (405 amino acids P32929, CGL_HUMAN Cystathionine gamma-lyase ; www.uniprot.org) using T-COFFEE (Version_11.00.d625267). Stars indicated identical amino acids among *C. elegans* CTH-2 and human CTH.

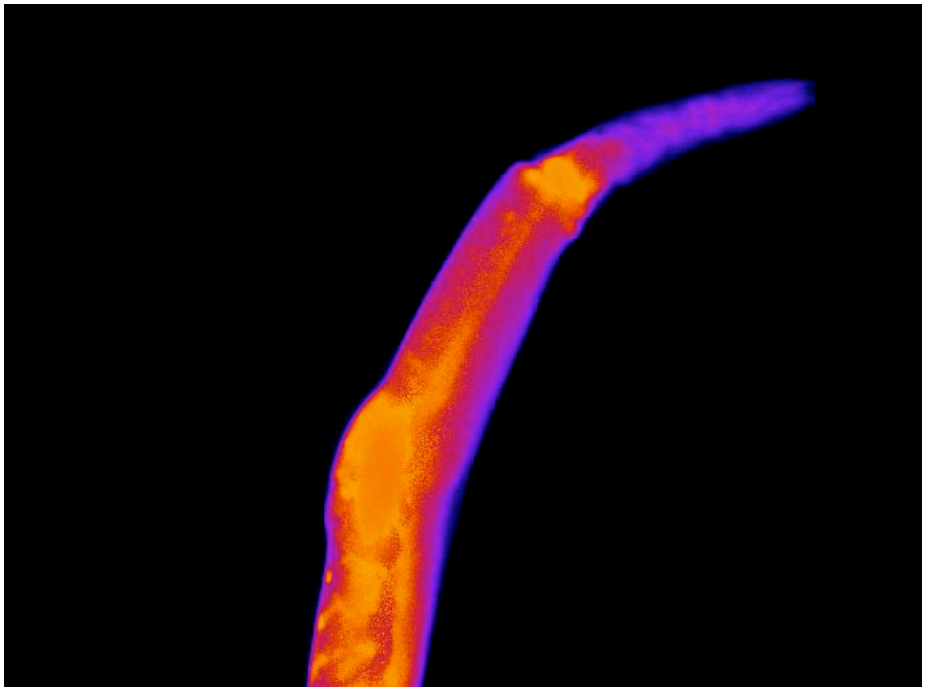

Supplementary Video 1: 3D image of persulfidation levels of wild type (N2). Worms were stained for protein persulfidation using dimedone-switch method and Cy5 signal recorded on epifluorescence microscope. Z-stack images were taken, deconvoluted and 3D image of PSSH levels generated.

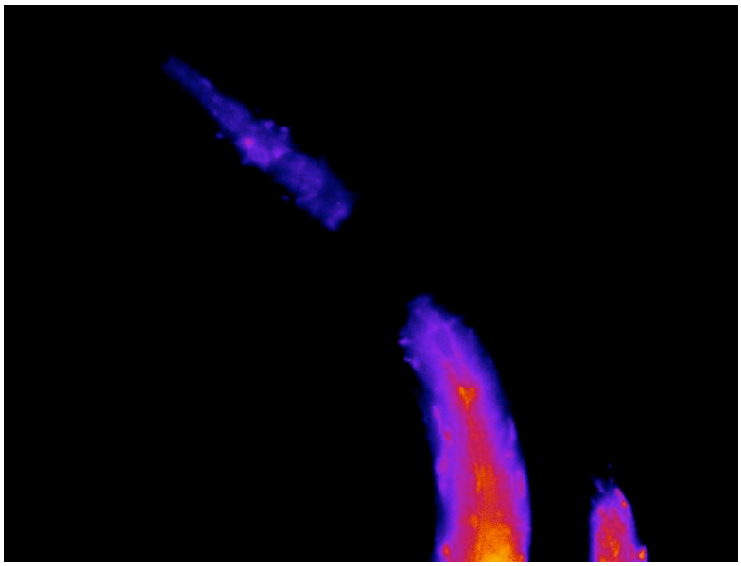

Supplementary Video 2: 3D image of persulfidation levels of *cth-2(mg599)* mutant. Worms were stained for protein persulfidation using dimedone-switch method

816 and Cy5 signal recorded on epifluorescence microscope. Z-stack images were taken,

817 deconvoluted and 3D image of PSSH levels generated.

818

Materials and Methods

Strains

Caenorhabditis elegans strains were maintained on NGM plates and OP50 *Escherichia coli* bacteria. The wild-type strain was N2 Bristol. Mutant strains used are described at www.wormbase.org: LGI: *eif-2a(qd338);* LGII: *cth-2(mg599), raga-1(ok386), spe-9(hc88), rrf-3(pk1426* and *b26), eat-2(ad1116), rict-1(ft7)*; LGIII: *rars-1(gc47), daf-2(e1368, e1370), glp-1(e2141), clk-1(qm30)*; LGX: *atf-4(tm4397, tm4212)*. Transgenic strains: LD1499 [P*atf-4*(uORF)::GFP::*unc-54*(3'UTR)] was made by Chi Yun (1.8kb promoter 5' of *atf-4* including both uORFs into pPD95.75, personal communication with Chi Yun and David Ron) [63].

Generation of transgenic lines

Construction of a translational fusion of ATF-4 with GFP. The plasmid pWM48 (P*atf-4*::ATF-4(gDNA)::GFP::*unc-54*(3'UTR)) was generated by introducing the 1.8kb promoter region 5' of *atf-4* and the *atf-4* genomic sequence into pAD1. This construct was used to generate two independent transgenic lines: *wbmEx26* [pWM48 (P*atf-4*::ATF-4(gDNA)::GFP::*unc-54*(3'UTR), pRF4 (*rol-6(su1006)*)] and *wbmEx27* [pWM48 (P*atf-4*::ATF-4(gDNA)::GFP::*unc-54*(3'UTR), pRF4 (*rol-6(su1006)*)]. UV irradiation was used for integration resulting in *ldIs119* from *wbmEx26* and *ldIs120-1* from *wbmEx27*, which were outcrossed 8-10x against N2.

Genomic organisation and alignments

The *atf-4* genomic representation was made using Exon-Intron Graphic Maker (http://wormweb.org/exonintron) from Nikhil Bhatla. DNA and mRNA sequences were

from www.wormbase.org (WS258). For human *ATF4* GenBank BC008090 mRNA sequence was used. The uORFs were predicted with ApE- A plasmid Editor v2.0.50b3. For amino acid alignments T-COFFEE (Version_11.00.d625267) was used.

Ribosome profiling analysis

Ribosome profiling sequencing data were downloaded from the NCBI Sequence Read Archive (S.R.A.) (http://www.ncbi.nlm.nih.gov/sra/) under accession number SRA055804. Data were analysed as the paper described [61]: Data analysis was performed with the help of Unix-based software tools. First, the quality of raw sequencing reads was determined by FastQC (Andrews, S. FastQC (Babraham Bioinformatics, 2010)). Reads were then filtered according to quality via FASTQ for a mean PHRED quality score above 30 [64]. Filtered reads were mapped to the worm reference genome (Wormbase WS275) using B.W.A. (version 0.7.5), and S.A.M. files were converted into B.A.M. files by SAMtools (version 0.1.19). Coverage data for specific genes (including 5'UTR, exons and 3'UTR) were calculated by SAMtools. The coverage data for each gene were plotted using R [65].

Knockdown by RNA interference

RNAi clones were from the Vidal and Ahringer RNAi libraries [66,67]. RNAi bacteria cultures were grown overnight in LB with carbenicillin [100 μg/ml] and tetracycline [12.5 μg/ml], diluted to an OD600 of 1, and induced with 1 mM IPTG and spread onto NGM plates containing tetracycline [12.5 μg/ml] and ampicillin [50 μg/ml]. For empty RNAi vector (EV) plasmid pL4440 was used as control.

867

868 **Manual lifespan assays**

869 Adult lifespan was determined either with or without 5-Fluoro-2'deoxyuridine (FUdR)
870 as described in Ewald and colleagues [68]. In brief, about 100 L4 *C. elegans* per strain
871 were picked onto NGM plates containing OP50 bacteria. The next day, *C. elegans*
872 (day-1-adults) were transferred onto either NGM plates containing 400 μM FUdR and
873 OP50 bacteria or RNAi bacteria. For cycloheximide-treatment lifespan, day-1-adults
874 were transferred on NGM OP50 plates either containing the solvent 0.25% dimethyl
875 sulfoxide (DMSO) alone as a control or cycloheximide (Sigma #C7698) dissolved in
876 0.25% DMSO. The rapamycin lifespan and liquid dietary restriction lifespans were
877 performed as described in [14] and [69], respectively. Animals were classified as dead if
878 they failed to respond to prodding. Exploded, bagged, burrowed, or animals that left
879 the agar were excluded from the statistics. The estimates of survival functions were
880 calculated using the product-limit (Kaplan-Meier) method. The log-rank (Mantel-Cox)
881 method was used to test the null hypothesis and calculate *P* values (JMP software
882 v.9.0.2.).

883

884 **Pharyngeal Pumping**

885 Pharyngeal pumping was assessed as described in [25]. In brief, pharyngeal pumping
886 was determined by counting grinder movements in 45 second intervals when the
887 animals were in the bacterial lawn and feeding.

888

889 **Quantitative Real-Time Polymerase Chain Reaction (qRT-PCR) Assays**

RNA was isolated with Trizol (TRI REAGENT Sigma), DNAse-treated, and cleaned over a column (RNA Clean & Concentrator™ ZYMO Research). First-strand cDNA was synthesised in duplicate from each sample (Invitogen SuperScript III). SYBR green was used to perform qRT-PCR (ABI 7900). For each primer set, a standard curve from genomic DNA accompanied the duplicate cDNA samples. mRNA levels relative to WT control were determined by normalising to the number of *C. elegans* and the geometric mean of three reference genes (*cdc-42, pmp-3,* and Y45F10D.4). At least two independent biological replicates were examined for each sample. For statistical analysis, one-sample *t*-test, two-tailed, a hypothetical mean of 1 was used for comparison using Prism 6.0 software (GraphPad).

RNA sequencing

Three independent biological replicates were prepared by using sodium hypochlorite to harvest eggs and overnight L1 arrest in M9 buffer with 10 μg/ml cholesterol to synchronise *C. elegans*. For each sample, about 20000 *C. elegans* per strain were allowed to develop to the L4 stage under normal growth conditions on NGM OP50 plates at 20°C (about 1000 *C. elegans* per one 10 cm NGM OP50 plate). WT, *atf-4(tm4397)*, and *ldIs119* were grown at the same time for each biological replicate. *C. elegans* were washed from the culturing NGM plates and washed additional 3 times with M9 buffer to wash away the OP50 bacteria. RNA was isolated with Trizol (TRI REAGENT Sigma), DNAse-treated, and cleaned over a column (RNA Clean & Concentrator™ ZYMO Research). The RNA was sent to Dana-Farber Cancer Institute Center for Computational Biology (CCCB, http://cccb.dfci.harvard.edu/rna-sequence). At the CCCB, the RNA Integrity Number (RIN) was assessed by using the Bioanalyzer

914 2100 (Agilent Technologies), and only samples with a high RIN score were used to
915 prepare cDNA libraries. All nine samples were multiplexed in a single lane. Single read
916 50 bp RNA-sequencing with poly(A) enrichment was performed using a HiSeq 2000
917 (Illumina). We aligned the FASTQ output files to the *C. elegans* WBcel235 reference
918 genome using STAR 2.4.0j software [70] with an average >80% coverage mapping the
919 reads to the genome. The differential gene expression analysis was performed using
920 Bioconductor (http://bioconductor.org) as described in [71]. Rsubread 1.16.1
921 featureCounts was used to quantify the mapped reads in the aligned SAM output files.
922 Transcripts with <1 count per million reads were discarded. Counts were scaled to
923 Reads Per Kilobase of transcript per Million mapped reads (RPKM) and deposited as
924 a final output file in (Supplementary Table 3). To analyse the differential expressed
925 genes, we compared *atf-4(tm4397)*, and *ldIs119* to wild type using Degust
926 (http://degust.erc.monash.edu) with the following settings: RPKM with minimum 5
927 counts using edgeR with a false discovery rate (FDR) of 0.1 and an absolute log fold
928 change (FC) of 1 relative to wild type. Results are displayed in MA-plots. Functional
929 annotation clustering was performed with DAVID[54] using high classification
930 stringencies.
931
932 **Analysis of RNA sequencing comparing with mammalian ATF4 orthologues**
933 The RNA-sequencing data described in the previous section was subjected to
934 differential expression analysis using the limma package (Smyth, Gordon K. "Limma:
935 linear models for microarray data." Bioinformatics and computational biology solutions
936 using R and Bioconductor. Springer, New York, NY, 2005. 397-420) available in the
937 programming language R (Team, R. Core. "R: A language and environment for

938 statistical computing." (2013): 201). The 200 most-upregulated genes that were
939 identified by comparison of ATF4 OE to WT and passed a Benjamini-Hochberg
940 adjusted *P*-value threshold of 0.1 were analysed further. Mammalian ATF4-specific
941 gene targets were obtained from Quiros et al. 2017 [29] and subjected to Ortholist2 to
942 infer *C. elegans* orthologs based on a comparative genomic meta-analysis [72]. The
943 intersection of the most-upregulated genes in our ATF4 OE to WT expression analysis
944 and the orthologs of the mammalian ATF4 targets is depicted as a heatmap showing
945 all biological replicates (#1-3) [73]. The *atf-4* mutant samples are shown separately since
946 the displayed genes were selected based on the comparison between ATF4 OE and
947 WT The absolute expression levels are displayed in a blue (low) to white (medium) to
948 red (high) color gradient, with genes indicated as gene names or sequence names if
949 the former is not available. Hierarchical clustering was applied to both genes (rows)
950 and samples (columns). Additional information: GO term enrichment yielded a
951 significant (P=0.047, Benjamini-Hochberg corrected) enrichment of the membrane raft
952 compartment (*lec-2, lec-4, lec-5*) while no significant enrichment for GO biological
953 process, GO molecular function, KEGG- or REACTOME pathways were found[57,58].
954
955 **CTH expression levels in mice**
956 Publicly-available expression datasets were analysed to quantify the change of CTH
957 expression levels in long-lived compared to normal-lived mice. A selected subset of
958 comparisons displaying CTH upregulation in longevity is depicted in Fig. 6b, while the
959 full table is provided in Supplementary Table 11. Microarray datasets and platform
960 information were obtained from GEO (https://www.ncbi.nlm.nih.gov/geo/) followed by
961 mapping probes to their corresponding genes and sequencing information was

obtained from SRA (https://www.ncbi.nlm.nih.gov/sra) and processed using Trim Galore (https://www.bioinformatics.babraham.ac.uk/projects/trim_galore/) and Salmon [74]. Datasets were centred and scaled, and subsequently, the mean fold change, as well as its standard error, were computed for the CTH gene.

Manual thermotolerance assays

Day-1-adults were placed on NGM OP50 plates (maximum 20 *C. elegans* per plate) and placed at 35ºC. Survival was scored every hour. Animals were classified as dead if they failed to respond to prodding. Exploded animals or animals that moved up on the side of the plate were censored from the analysis. The estimates of survival functions were calculated using the product-limit (Kaplan-Meier) method. The log-rank (Mantel-Cox) method was used to test the null hypothesis and calculate *P* values (JMP software v.9.0.2.).

Automated survival assays using the lifespan machine

Automated survival analysis was conducted using the lifespan machine described by Stroustrup and colleagues [75]. Approximately 500 L4 animals were resuspended in M9 and transferred to NGM plates containing 50 μM 5-Fluoro-2'deoxyuridine (FUdR) seeded either with OP50 bacteria, or with RNAi bacteria supplemented with 100 µg/ml carbenicillin, or with heat-killed OP50 bacteria, or with UV-inactivated *E. coli* strain NEC937 B (OP50 ΔuvrA; KanR) containing 100 µg/ml carbenicillin. For oxidative stress assays, tBOOH was added to 2 mM to the NGM immediately before pouring, and seeding with heat-killed OP50 bacteria. Animals were kept at 20°C until measurement. Heat and oxidative stress experiments were performed using regular

petri dishes sealed with parafilm, while tight-fitting petri dishes (BD Falcon Petri Dishes, 50x9mm) were used for lifespan experiments. Tight-fitting plates were dried without lids in a laminar flow hood for 40 minutes before starting the experiment. Air-cooled Epson V800 scanners were utilised for all experiments operating at a scanning frequency of one scan per 10 - 30 minutes. Temperature probes (Thermoworks, Utah, U.S.) were used to monitor the temperature on the scanner flatbed and maintain 20°C constantly. Animals which left the imaging area during the experiment were censored. Population survival was determined using the statistical software R [65] with the survival [76] and survminer (https://rpkgs.datanovia.com/survminer/) packages. Lifespans were calculated from the L4 stage (= day 0). For stress survival assays the moment of exposure was utilised to define the time point zero of each experiment.

Manual oxidative stress assay (arsenite and tBHP)

The manual oxidative stress assays were performed as described in detail in the bio-protocol [77].

Oxidative stress assay by quantifying movement in arsenite

C. elegans were collected from NGM plates and washed four times by centrifugation, aspirating the supernatant and resuspending in fresh M9 buffer again. After the final wash, the supernatant was removed, and 10 µl of the *C. elegans* suspension pipetted into each well of a round-bottom 96-well microplate resulting in approximately 40 - 70 animals per well. To prevent desiccation, the wells were filled up immediately with either 30 µl M9, or 30 µl M9 containing 6.7 mM or 18.7 mM sodium arsenite yielding a final arsenite concentration of 0, 5, or 14 mM, respectively. Per *C. elegans* strain and

conditions, we loaded two wells with M9 as control and six wells with either 5 or 14 mM arsenite as technical replicates. The plate was closed, sealed with Parafilm and briefly stirred and then loaded into the wMicrotracker device (NemaMetrix). Data acquisition was performed for 50 hours, according to the manufacturer's instructions. The acquired movement dataset was analysed using the statistical programming language R.

Hydrogen sulfide capacity assay

The H_2S capacity assay was adapted from Hine and colleagues [35]. *C. elegans* were harvested from NGM plates and washed four times by centrifugation and resuspension with M9 to remove residual bacteria. Approximately 3000 animals were collected as a pellet and mixed with the same volume of 2x passive lysis buffer (Promega, E194A) on ice. Three freeze-thaw cycles were performed by freezing the samples in liquid nitrogen and thawing them again using a heat block set to 37°C. Particles were removed by centrifuging at 12000 g for 10 minutes at 4°C. The pellet was discarded, and the supernatant used further. The protein content of each sample was determined (BCA protein assay, Thermo scientific, 23225) and the sample sequentially diluted with distilled water to the required protein mass range, usually 25 - 200 μg protein. To produce the lead acetate paper, we submerged chromatography paper (Whatman paper 3M (GE Healthcare, 3030-917)) in a 20 mM lead acetate (Lead (II) acetate trihydrate (Sigma, 215902-25G)) solution for one minute and then let it dry overnight. The fuel mix was prepared freshly by mixing Pyridoxal 5′-phosphate hydrate (Sigma, P9255-5G) and L-Cysteine (Sigma, C7352-25G) in Phosphate Buffered Saline on ice at final concentrations of 2.5 mM and 25 mM, respectively. A

96-well plate was placed on ice, 80 µl of each sample were loaded into each well and mixed with 20 µl fuel mix and subsequently covered using the lead acetate paper. The assay plate was then incubated at 37°C for 3 hours under a weight of approximately 1 kg to keep the lead acetate paper firmly in place. For analysis, the exposed lead acetate paper was imaged using a photo scanner.

H_2S production capacity in liver homogenates: flash frozen liver was homogenised in passive lysis buffer (Promega, PLB E1941) and volume normalised to protein content. 100 µg of protein was added to a final reaction in 96-well format containing PBS, 1 mM Pyridoxal 5′-phosphate and 10 mM Cys, covered using the lead acetate paper. The assay plate was then incubated at 37°C for 1-2 hours under a weight of approximately 1 kg to keep the lead acetate paper firmly in place, with the paper incubated until a detectable, but non-saturated signal was seen. Quantification of H_2S production was performed by measuring the integrated density using ImageJ, compared to a well next to it that contained no protein for background.

In-gel persulfidation assay

Synchronous populations of embryos were obtained by lysing gravid hermaphrodites in alkaline bleach as previously described [78]. After they were washed free of bleach by centrifugation, the embryos were put on standard NGM agar plates seeded with *E. coli OP50-1*, ~4000 embryos/plate. At Day-1 adult stage *C. elegans* of different strains were collected from the NGM plates, 4 plates/strain, into 15 ml falcon tubes using M9 buffer and washed three times. Worm pellets were frozen in liquid nitrogen and 500 µl of glass beads was added in every tube. Samples were put in the bead beater (FastPrep-24, MP Biomedicals, California, U.S.A.) for 35 seconds at speed 6.5 m/s,

followed by an additional cycle at the same speed for 20 seconds. HEN lysis buffer supplemented with 1% protease inhibitor and 20 mM NBF-Cl was added to each tube, and centrifuged for 15 min at 13000 rpm at 4°C. Supernatants were collected and incubated at 37 °C for 45 min. Samples were then precipitated and protein pellets were switch labelled for persulfides and processed as previously described [37].

Persulfidation levels by fluorescence microscopy

The worms were fixed with 4% paraformaldehyde in Eppendorf tubes, washed with PBS, and frozen in liquid nitrogen to freeze-crack the cuticle. Worms were then stained, first with 1 mM (final concentration) 4-chloro-7-nitrobenzofurazane for 1 hr at 37 °C, then washed with PBS/Triton X100 (0.1%) 3 times, and incubated with 10 µM (final concentrations) DAz-2:Cy-5 click mix for 1 hr at 37 °C [37]. For the negative control worms were incubated with 10 µM DAz-2:Cy-5 click mix prepared without DAz-2. After overnight washing with PBS, worms were washed with methanol 3 x 10 min, followed by an additional washing with PBS. *Z*-stack images were taken on Olympus IX81 inverted fluorescence microscope using x 100 oil objective lens; images were then deconvoluted and 3D pictures generated using ImageJ software (NIH).

Scoring of transgenic promoter-driven GFP

For P*atf-4*(uORF)::GFP, L4 stage transgenic animals were exposed to chemicals by top-coating with 500 µl of each reagent (alpha-amanitin (Sigma #A2263), cycloheximide (Sigma #C7698), tunicamycin (Sigma #T7765), sodium arsenite (Honeywell International #35000)) or control (DMSO or M9 buffer) onto 6 cm NGM OP50 plates for 30 min to 4 hours, except that rapamycin (LC laboratories) was added

to the NGM agar as described [14,25]. Then GFP fluorescent levels were either (1) scored or (2) quantified. (1) *GFP scoring*: Transgenic animals were first inspected with a dissecting scope while on still on the plate. GFP intensity was scored in the following categories: 0= none or very low GFP usually corresponding to untreated control, 1= low, 2= medium, and 3= high GFP fluorescence visible. Animals were either washed off chemical treated plates, washed again at least twice, placed on OP50 NGM plates and were picked from there and mounted onto slides and GFP fluorescence was scored using a Zeiss AxioSKOP2 or a Tritech Research BX-51-F microscope with optimised triple-band filter-sets to distinguish autofluorescence from GFP at 40x as described [79]. GFP was scored as the following: None: no GFP (excluding spermatheca), low: either only anterior or only posterior of the animal with weak GFP induction, Medium: both anterior and posterior of the animal with GFP but no GFP in the middle of the animal. High: GFP throughout the animal. *P* values were determined by Chi^2 test. (2) *Quantification of GFP fluorescent levels*: Animals were washed off reagent-containing plates, washed an additional two times, then placed into 24-well plates containing 0.06% tetramisole dissolved in M9 buffer to immobilise animals. Fluorescent pictures were taken with the same exposure settings (1s) at 10x magnification using an Olympus Cellsens Standard Camera on an inverted microscope. GFP levels were assessed by drawing a line around the animal, measuring mean grey value and using the same area next to it for background using ImageJ. The arbitrary fluorescent value corresponds to mean grey value of the animals minus the background.

Western blot

About 5000 *C. elegans* (L4 or day-1-adults indicated in figure legends) were sonicated in lysis buffer (RIPA buffer (ThermoFisher #89900), 20 mM sodium fluoride (Sigma #67414), 2 mM sodium orthovanadate (Sigma #450243), and protease inhibitor (Roche #04693116001)) and kept on ice for 15 min before being centrifuged for 10 min at 15'000 x g. For equal loading, the protein concentration of the supernatant was determined with BioRad DC protein assay kit II (#5000116) and standard curve with Albumin (Pierce #23210). Samples were treated at 95°C for 5 min, centrifuged for 1 min at 10'000 x g and 40 μg protein was loaded onto NuPAGE Bis-Tris 10% Protein Gels (ThermoFisher #NP0301BOX), and proteins were transferred to nitrocellulose membranes (Sigma #GE10600002). Western blot analysis was performed under standard conditions with antibodies against Tubulin (1:500, Sigma #T9026), GFP (1:1'000, Roche #11814460001), Cystathionase/CTH (1:2000, abcam #ab151769) and Phospho-eIF2alpha (Ser51) (1:1'000, CellSignal #9721). HRP-conjugated goat anti-mouse (1:2'000, Cell Signaling #7076) and goat anti-rabbit (1:2'000, Cell Signaling #7074) secondary antibodies were used to detect the proteins by enhanced chemiluminescence (Bio-Rad #1705061). For loading control (*i.e.,* Tubulin) either corresponding samples were run in parallel or membrane was cut if the size of Tubulin and protein of interest were not overlapping, or the blot was stripped (indicated in figure legends). For stripping, membranes were incubated for 5 min in acid buffer (0.2 M Glycin, 0.5 M NaCl, pH set to 2 with HCl) and afterwards for 10 min in basic buffer (0.5 M Tris, pH set to 11 with NaOH) and washed with TBS-T before blocking. Quantification of protein levels was determined by densitometry using ImageJ software and normalised to loading control (*i.e.*, Tubulin).

Mouse work

All mouse experiments were performed with the approval of the Local University Institutional Animal Care and Use Committee (IACUC). 8 to 14-week-old male or female C57BL/6 mice (The Jackson Laboratory, Bar Harbor, ME) were used for all experiments unless otherwise indicated. Except where indicated, animals were maintained under standard group housing conditions with ad libitum (AL) access to food (Purina 5058) and water, 12-hr light/12-hr dark cycles, temperature between 20 - 23°C with 30% - 70% relative humidity. AL food intake/g body weight was monitored daily for several days and used to calculate calorie restriction (CR) based on initial animal weights. Animals were fed daily with fresh food between 6 - 7 PM. Adenoviral-mediated gene delivery: Knockdown of ATF4 was accomplished by IV injection of IV injection of1010 PFUs of an adenovirus-type 5 (dE1/E3) containing the CMV promoter driving the expression of a shRNA for silencing of Mouse Atf4, Ad-m-ATF4-shRNA, or the negative control virus Ad-CMV Null adenovirus amplified and purified by Vector Biolabs (Philadelphia, PA, U.S.A.).

References

Note: Reference 1-60 for main text, 61-79 are references from detailed Materials and Methods

1. Kenyon, C. J. The genetics of ageing. *Nature* **464**, 504–512 (2010).

2. Blackwell, T. K., Sewell, A. K., Wu, Z. & Han, M. TOR Signaling in Caenorhabditis elegans Development, Metabolism, and Aging. *Genetics* **213**, 329–360 (2019).

3. Liu, G. Y., Liu, G. Y. & Sabatini, D. M. mTOR at the nexus of nutrition, growth, ageing and disease. *Nature Reviews Molecular Cell Biology* **21**, 183–203 (2020).

4. Cornu, M., Albert, V. & Hall, M. N. mTOR in aging, metabolism, and cancer. *Current opinion in genetics & development* **23**, 53–62 (2013).

5. López-Otín, C., Blasco, M. A., Partridge, L., Serrano, M. & Kroemer, G. The hallmarks of aging. *Cell* **153**, 1194–1217 (2013).

6. Antikainen, H., Driscoll, M., Haspel, G. & Dobrowolski, R. TOR-mediated regulation of metabolism in aging. *Aging cell* **16**, 1219–1233 (2017).

7. Johnson, S. C., Rabinovitch, P. S. & Kaeberlein, M. mTOR is a key modulator of ageing and age-related disease. *Nature* **493**, 338–345 (2013).

8. Pan, K. Z., Palter, J. E., Lithgow, G. J. & Kapahi, P. Inhibition of mRNA translation extends lifespan in Caenorhabditis elegans. *Aging cell* **6**, 111–119 (2007).

9. Curran, S. P. & Ruvkun, G. Lifespan regulation by evolutionarily conserved genes essential for viability. *PLoS genetics* **3**, e56 (2007).

10. Syntichaki, P., Troulinaki, K. & Tavernarakis, N. eIF4E function in somatic cells modulates ageing in Caenorhabditis elegans. *Nature* **445**, 922–926 (2007).

11. Wang, J. *et al.* RNAi screening implicates a SKN-1-dependent transcriptional response in stress resistance and longevity deriving from translation inhibition. *PLoS genetics* **6**, e1001048 (2010).

12. Howard, A. C., Rollins, J., Snow, S., Castor, S. & Rogers, A. N. Reducing translation through eIF4G/IFG-1 improves survival under ER stress that depends on heat shock factor HSF-1 in Caenorhabditis elegans. *Aging cell* **15**, 1027–1038 (2016).

13. Hansen, M. *et al.* Lifespan extension by conditions that inhibit translation in Caenorhabditis elegans. *Aging Cell* **6**, 95–110 (2007).

14. Robida-Stubbs, S. *et al.* TOR signaling and rapamycin influence longevity by regulating SKN-1/Nrf and DAF-16/FoxO. *Cell metabolism* **15**, 713–724 (2012).

1178 15. Bjedov, I. *et al.* Mechanisms of life span extension by rapamycin in the fruit fly
1179 Drosophila melanogaster. *Cell metabolism* **11**, 35–46 (2010).

1180 16. Harding, H. P. *et al.* An Integrated Stress Response Regulates Amino Acid Metabolism
1181 and Resistance to Oxidative Stress. *Mol Cell* **11**, 619–633 (2003).

1182 17. Pakos-Zebrucka, K. *et al.* The integrated stress response. *EMBO reports* **17**, 1374–1395
1183 (2016).

1184 18. Costa-Mattioli, M. & Walter, P. The integrated stress response: From mechanism to
1185 disease. *Science (New York, NY)* **368**, (2020).

1186 19. Park, Y., Reyna-Neyra, A., Philippe, L. & Thoreen, C. C. mTORC1 Balances Cellular
1187 Amino Acid Supply with Demand for Protein Synthesis through Post- transcriptional Control
1188 of ATF4. *Cell reports* **19**, 1083–1090 (2017).

1189 20. Ben-Sahra, I., Hoxhaj, G., Ricoult, S. J. H., Asara, J. M. & Manning, B. D. mTORC1
1190 induces purine synthesis through control of the mitochondrial tetrahydrofolate cycle. *Science*
1191 *(New York, NY)* **351**, 728–733 (2016).

1192 21. Selvarajah, B. *et al.* mTORC1 amplifies the ATF4-dependent de novo serine-glycine
1193 pathway to supply glycine during TGF-β 1 –induced collagen biosynthesis. *Sci Signal* **12**,
1194 eaav3048 (2019).

1195 22. Wek, R. C. & Cavener, D. R. Translational control and the unfolded protein response.
1196 *Antioxidants & Redox Signaling* **9**, 2357–2371 (2007).

1197 23. Rousakis, A. *et al.* The general control nonderepressible-2 kinase mediates stress
1198 response and longevity induced by target of rapamycin inactivation in Caenorhabditis
1199 elegans. *Aging cell* **12**, 742–751 (2013).

1200 24. Blackwell, T. K., Steinbaugh, M. J., Hourihan, J. M., Ewald, C. Y. & Isik, M. SKN-1/Nrf,
1201 stress responses, and aging in Caenorhabditis elegans. *Free radical biology & medicine* **88**,
1202 290–301 (2015).

1203 25. Ewald, C. Y., Landis, J. N., Abate, J. P., Murphy, C. T. & Blackwell, T. K. Dauer-
1204 independent insulin/IGF-1-signalling implicates collagen remodelling in longevity. *Nature*
1205 **519**, 97–101 (2015).

1206 26. Hsu, A.-L., Murphy, C. T. & Kenyon, C. J. Regulation of aging and age-related disease
1207 by DAF-16 and heat-shock factor. *Science (New York, NY)* **300**, 1142–1145 (2003).

1208 27. Oliveira, R. P. *et al.* Condition-adapted stress and longevity gene regulation by
1209 Caenorhabditis elegans SKN-1/Nrf. *Aging cell* **8**, 524–541 (2009).

1210 28. Molenaars, M. *et al.* A Conserved Mito-Cytosolic Translational Balance Links Two
1211 Longevity Pathways. *Cell metabolism* **31**, 549-563.e7 (2020).

29. Quiros, P. M. *et al.* Multi-omics analysis identifies ATF4 as a key regulator of the mitochondrial stress response in mammals. *The Journal of cell biology* **216**, 2027–2045 (2017).

30. Hoshino, A. *et al.* The ADP/ATP translocase drives mitophagy independent of nucleotide exchange. *Nature* **575**, 375–379 (2019).

31. Han, J. *et al.* ER-stress-induced transcriptional regulation increases protein synthesis leading to cell death. *Nature Cell Biology* **15**, 481–490 (2013).

32. Zhu, J. *et al.* Transsulfuration Activity Can Support Cell Growth upon Extracellular Cysteine Limitation. *Cell metabolism* **30**, 865-876.e5 (2019).

33. Miller, R. A. & Harper, J. M. Methionine-deficient diet extends mouse lifespan, slows immune and lens aging, alters glucose, T4, IGF-I and insulin levels, and increases hepatocyte MIF levels and stress resistance. *Aging cell* **4**, 119–125 (2005).

34. Miller, D. L. & Roth, M. B. Hydrogen sulfide increases thermotolerance and lifespan in Caenorhabditis elegans. *Proc National Acad Sci* **104**, 20618–20622 (2007).

35. Hine, C. *et al.* Endogenous Hydrogen Sulfide Production Is Essential for Dietary Restriction Benefits. *Cell* **160**, 132–144 (2015).

36. Walter, P. & Ron, D. The unfolded protein response: from stress pathway to homeostatic regulation. *Science (New York, NY)* **334**, 1081–1086 (2011).

37. Zivanovic, J. *et al.* Selective Persulfide Detection Reveals Evolutionarily Conserved Antiaging Effects of S-Sulfhydration. *Cell metabolism* **30**, 1152-1170.e13 (2019).

38. Lamming, D. W. *et al.* Rapamycin-induced insulin resistance is mediated by mTORC2 loss and uncoupled from longevity. *Science (New York, NY)* **335**, 1638–1643 (2012).

39. Oppliger, W. & Hall, M. N. Activation of mTORC2 by association with the ribosome. *Cell* **144**, 757–768 (2011).

40. Jones, K. T., Greer, E. R., Pearce, D. & Ashrafi, K. Rictor/TORC2 regulates Caenorhabditis elegans fat storage, body size, and development through sgk-1. *PLoS Biology* **7**, e60 (2009).

41. Mizunuma, M., Neumann-Haefelin, E., Moroz, N., Li, Y. & Blackwell, T. K. mTORC2-SGK-1 acts in two environmentally responsive pathways with opposing effects on longevity. *Aging cell* **13**, 869–878 (2014).

42. Zhou, B. *et al.* Mitochondrial Permeability Uncouples Elevated Autophagy and Lifespan Extension. *Cell* **177**, 299-314.e16 (2019).

43. Filipovic, M. R., Zivanovic, J., Álvarez, B. & Banerjee, R. Chemical Biology of H2S Signaling through Persulfidation. *Chemical reviews* **118**, 1253–1337 (2018).

1246 44. Paul, B. D. & Snyder, S. H. H2S: A Novel Gasotransmitter that Signals by Sulfhydration.
1247 *Trends Biochem Sci* **40**, 687–700 (2015).

1248 45. Zhang, Y. *et al.* Neuronal TORC1 modulates longevity via AMPK and cell
1249 nonautonomous regulation of mitochondrial dynamics in C. elegans. *Elife* **8**, e49158 (2019).

1250 46. Harrison, D. E. *et al.* Rapamycin fed late in life extends lifespan in genetically
1251 heterogeneous mice. *Nature* **460**, 392–395 (2009).

1252 47. Longchamp, A. *et al.* Amino Acid Restriction Triggers Angiogenesis via GCN2/ATF4
1253 Regulation of VEGF and H2S Production. *Cell* **173**, 117-129.e14 (2018).

1254 48. Tyshkovskiy, A. *et al.* Identification and Application of Gene Expression Signatures
1255 Associated with Lifespan Extension. *Cell metabolism* **30**, 573-593.e8 (2019).

1256 49. Rogers, A. N. *et al.* Life span extension via eIF4G inhibition is mediated by
1257 posttranscriptional remodeling of stress response gene expression in C. elegans. *Cell*
1258 *metabolism* **14**, 55–66 (2011).

1259 50. Steffen, K. K. *et al.* Yeast life span extension by depletion of 60s ribosomal subunits is
1260 mediated by Gcn4. *Cell* **133**, 292–302 (2008).

1261 51. Li, W., Li, X. & Miller, R. A. ATF4 activity: a common feature shared by many kinds of
1262 slow-aging mice. *Aging cell* **13**, 1012–1018 (2014).

1263 52. Heintz, C. *et al.* Splicing factor 1 modulates dietary restriction and TORC1 pathway
1264 longevity in C. elegans. *Nature* **541**, 102–106 (2017).

1265 53. Lee, G. *et al.* Post-transcriptional Regulation of De Novo Lipogenesis by mTORC1-
1266 S6K1-SRPK2 Signaling. *Cell* **171**, 1545-1558.e18 (2017).

1267 54. Wu, L. *et al.* An Ancient, Unified Mechanism for Metformin Growth Inhibition in
1268 C. elegans and Cancer. *Cell* **167**, 1705-1718.e13 (2016).

1269 55. Sidrauski, C. *et al.* Pharmacological brake-release of mRNA translation enhances
1270 cognitive memory. *eLife* **2**, e00498 (2013).

1271 56. Paul, B. D. & Snyder, S. H. H_2S signalling through protein sulfhydration and beyond.
1272 *Nature Reviews Molecular Cell Biology* **13**, 499–507 (2012).

1273 57. Yang, G. *et al.* H2S as a physiologic vasorelaxant: hypertension in mice with deletion of
1274 cystathionine gamma-lyase. *Science (New York, NY)* **322**, 587–590 (2008).

1275 58. Longchamp, A. *et al.* Hydrogen sulfide-releasing peptide hydrogel limits the development
1276 of intimal hyperplasia in human vein segments. *Acta biomaterialia* **97**, 374–384 (2019).

1277 59. Wang, Y. *et al.* Role of hydrogen sulfide in the development of atherosclerotic lesions in
1278 apolipoprotein E knockout mice. *Arteriosclerosis, thrombosis, and vascular biology* **29**, 173–
1279 179 (2009).

1280 60. Islam, K. N., Polhemus, D. J., Donnarumma, E., Brewster, L. P. & Lefer, D. J. Hydrogen
1281 Sulfide Levels and Nuclear Factor-Erythroid 2-Related Factor 2 (NRF2) Activity Are
1282 Attenuated in the Setting of Critical Limb Ischemia (CLI). *Journal of the American Heart*
1283 *Association* **4**, (2015).

1284 61. Stadler, M., Artiles, K., Pak, J. & Fire, A. Contributions of mRNA abundance, ribosome
1285 loading, and post- or peri-translational effects to temporal repression of C. elegans
1286 heterochronic miRNA targets. *Genome research* **22**, 2418–2426 (2012).

1287 62. Fiorese, C. J. *et al.* The Transcription Factor ATF5 Mediates a Mammalian Mitochondrial
1288 UPR. *Current biology : CB* **26**, 2037–2043 (2016).

1289 63. Venz, R., Korosteleva, A., Jongsma, E. & Ewald, C. Y. Combining Auxin-Induced
1290 Degradation and RNAi Screening Identifies Novel Genes Involved in Lipid Bilayer Stress
1291 Sensing in Caenorhabditis elegans. *G3 Genes Genomes Genetics* g3.401635.2020 (2020)
1292 doi:10.1534/g3.120.401635.

1293 64. Blankenberg, D. *et al.* Manipulation of FASTQ data with Galaxy. *Bioinformatics* **26**,
1294 1783–1785 (2010).

1295 65. Ihaka, R. & Gentleman, R. R: A Language for Data Analysis and Graphics. *J Comput*
1296 *Graph Stat* **5**, 299–314 (2012).

1297 66. Rual, J.-F. *et al.* Toward improving Caenorhabditis elegans phenome mapping with an
1298 ORFeome-based RNAi library. *Genome research* **14**, 2162–2168 (2004).

1299 67. Fraser, A. G. *et al.* Functional genomic analysis of C. elegans chromosome I by
1300 systematic RNA interference. *Nature* **408**, 325–330 (2000).

1301 68. Ewald, C. Y. *et al.* NADPH oxidase-mediated redox signaling promotes oxidative stress
1302 resistance and longevity through memo-1 in C. elegans. *eLife* **6**, 819 (2017).

1303 69. Moroz, N. *et al.* Dietary restriction involves NAD^+ -dependent mechanisms and a shift
1304 toward oxidative metabolism. *Aging cell* **13**, 1075–1085 (2014).

1305 70. Dobin, A. *et al.* STAR: ultrafast universal RNA-seq aligner. *Bioinformatics* **29**, 15–21
1306 (2013).

1307 71. Steinbaugh, M. J. *et al.* Lipid-mediated regulation of SKN-1/Nrf in response to germ cell
1308 absence. *eLife* **4**, (2015).

1309 72. Kim, W., Underwood, R. S., Greenwald, I. & Shaye, D. D. OrthoList 2: A New
1310 Comparative Genomic Analysis of Human and Caenorhabditis elegans Genes. *Genetics* **210**,
1311 445–461 (2018).

1312 73. Gu, Z., Eils, R. & Schlesner, M. Complex heatmaps reveal patterns and correlations in
1313 multidimensional genomic data. *Bioinform Oxf Engl* **32**, 2847–9 (2016).

1314 74. Patro, R., Duggal, G., Love, M. I., Irizarry, R. A. & Kingsford, C. Salmon provides fast
1315 and bias-aware quantification of transcript expression. *Nat Methods* **14**, 417–419 (2017).

1316 75. Stroustrup, N. *et al.* The Caenorhabditis elegans Lifespan Machine. *Nature Methods* **10**,
1317 665–670 (2013).

1318 76. Therneau, T. M. & Grambsch, P. M. Modeling Survival Data: Extending the Cox Model.
1319 1–6 (2000) doi:10.1007/978-1-4757-3294-8_1.

1320 77. Ewald, C. Y., Hourihan, J. M. & Blackwell, T. K. Oxidative Stress Assays (arsenite and
1321 tBHP) in Caenorhabditis elegans. *BIO-PROTOCOL* **7**, (2017).

1322 78. Teuscher, A. C., Statzer, C., Pantasis, S., Bordoli, M. R. & Ewald, C. Y. Assessing
1323 Collagen Deposition During Aging in Mammalian Tissue and in Caenorhabditis elegans.
1324 *Methods in molecular biology (Clifton, NJ)* **1944**, 169–188 (2019).

1325 79. Teuscher, A. C. & Ewald, C. Y. Overcoming Autofluorescence to Assess GFP
1326 Expression During Normal Physiology and Aging in Caenorhabditis elegans. *BIO-*
1327 *PROTOCOL* **8**, (2018).

1328